Quasi-periodic boundary conditions for hierarchical algorithms used for the calculation of inter-particle electrostatic interactions

Athanasios Boutsikakis, Pascal Fede, Olivier Simonin

Version of Record: https://www.sciencedirect.com/science/article/pii/S0021999122007495
Manuscript_29b2b49674cfbf355031ab35ba0003e9

Journal of Computational Physics (2022)

Contents lists available at ScienceDirect

Journal of Computational Physics

journal homepage: www.elsevier.com/locate/jcp

Quasi-periodic boundary conditions for hierarchical algorithms used for the calculation of inter-particle electrostatic interactions

Athanasios Boutsikakis [a,*], Pascal Fede[a], Olivier Simonin[a]

[a] *Institut de Mécanique des Fluides de Toulouse (IMFT), Université de Toulouse, CNRS, Toulouse, France*

ARTICLE INFO

Article history:
Received
Received in final form
Accepted
Available online

Keywords:
Particle flows
Charged particles
Electrostatic interaction
Hierarchical algorithms
Periodic boundary conditions

ABSTRACT

In the present work, a simplified way to apply tri-periodic Boundary Conditions (BCs) in hierarchical algorithms has been devised. The application of these BCs is demonstrated using an in-house algorithm that is used for the calculation of electrostatic interactions in a system of charged particles. The proposed quasi-periodic BCs entail a truncation of the infinite periodic domain with a reasonable cut-off error. For a correct representation of the physics, two properties have to be ensured: the convergence of the electrostatic forces and the isotropy of the electric field. The developed algorithm allows for a rather efficient and precise calculation of the former in a tri-periodic computational domain by separating them in short- and long-range parts, which are calculated exactly and approximately, respectively. The approximation error, computational cost and performance of the proposed algorithm are documented and thoroughly analyzed. Then, an application of the method is presented for dry mono-charged (all particles bear equal charge) particle flows where the fundamentals physics of particle-particle electrostatic interactions are investigated via characteristic length and time scales. It is shown that the underlying mechanism of these interactions is the Coulomb collision, a concept that allows to interpret these interactions in a rather intuitive way. In addition, an attempt is made to provide analytical estimations for several statistical quantities via dimensional analysis based on measured simulation data. Finally, the particle-induced electric field is presented and its characteristics are related to particle motion.

*Corresponding author
e-mail: aboutsik@imft.fr (Athanasios Boutsikakis)

1. Introduction

The motivation for this work comes from numerous practical applications of particle-laden flows where particles are electrically charged. The range of these applications is quite vast, including geophysical (pyroclastic flow, sediments transport, volcano ashes dispersion) and atmospheric flows (cloud formation, rain enhancement, fog elimination), industrial configurations(pneumatic conveying, olefin polymerization, Fluid Catalytic Cracking of oil, silo discharge), nano-material science, aerospace applications (space exploration, propulsion), biomolecular engineering (DNA charge clouds), chemical and pharmaceutical engineering (protein structure, coating techniques). Depending on the application, these interactions can be either an observed physical phenomenon or a choice of active/passive control of the flow. Most of the aforementioned applications, fall into the category of dispersed multiphase flows, as they usually include a carrier fluid phase (air, gas) and a dispersed solid particle phase that is transported by the former. The latter, can be also electrically charged, thus apart from the fluid-particle interaction, in this case the inter-particle electrostatic interactions play an important role in the particle flow dynamics.

The problem of predicting the individual motions of all N_p particles interacting with each other electrostatically falls into the category of an N-body problem. This problem has interested astronomers, physicists and mathematicians for the last several hundred years. It has, in fact, motivated much of the theoretical work done during that time, from cosmology to solid state physics to differential equations and potential theory. Unfortunately, the equations of motion of systems $N_p > 2$ do not allow for an analytical solution.

Until the mid 80s, theoretical studies have been limited to determining the coarse qualitative behavior of the system. With the introduction of high-speed computers, however, the calculation of trajectories of many particles in detail became feasible [1]. The equations of motion of a system of N_p particles are described by a set of N_p ordinary differential equations, each of which is simply Newton's second law of motion applied to an individual particle. It is clear that the amount of work required for moving all particles is proportional to N_p, but that the amount of work required for computing all forces is proportional to ${N_p}^2$, since it involves determining all dipole interactions. This quadratic growth in cost has been a major limitation on the size of the systems which can be handled, even by the fastest supercomputers.

In the 80s, a group of algorithms has been developed in the astrophysics community which have come to be known as "tree codes" or "hierarchical codes" [2, 3]. They are designed to work well in a variety of settings, including ones where there is a high degree of clustering. The basic idea is to replace groups of distant particles by their centers of mass, and to compute the interactions between groups via this approximation. Although some accuracy is generally sacrificed, the computational cost of these methods grows as $\mathcal{O}\left(N_p \log N_p\right)$ rather than $\mathcal{O}\left(N_p^2\right)$.

Along with the development of these tree codes, while working in fluid dynamics, [4] proposed a scheme for two-dimensional calculations which is also $\mathcal{O}\left(N_p \log N_p\right)$, but highly accurate. Although the physical intuition underlying their method is the same, the increased accuracy is obtained by the application of

asymptotic analysis. A closely related scheme, the Fast Multipole Method (FMM) has been developed by [5]. It is also highly accurate, as it involves a more elaborate asymptotic analysis and requires an amount of operations proportional to $\mathcal{O}(N_p)$.

In the 90s, significant progress was made in reducing the cost of the numerical calculation of forces acting at a distance, such as electrostatic forces. The first breakthrough, allowing simulations with orders of magnitude more bodies, came with the advent of the Particle-Mesh (PM) approach introduced by [6], which makes use of an underlying grid to speed up the evaluation of the long-range potential. An evolution of this method is the PPPM or P^3M method which consists in taking into account the short-range forces up to a certain inter-particle distance, while the long-range contributions are included by the particle-mesh procedure. The P^3M method requires modifying the long-range potential in Fourier space to avoid double counting the short- and long-range contributions and scales with $\mathcal{O}(N \log N)$. This type of methods are extremely efficient when the particle distribution is more or less uniform and the required precision is relatively low. However, a severe degradation of performance is observed when the bodies are clustered and when the required precision is high [7].

To handle long-range potentials accurately in periodic boxes, [8] developed the homonymous summation approach. It consists in splitting the Coulomb potential into short- and long-range contributions, each of which converges exponentially fast [9]. The fast converging short-range potential is evaluated using direct pairwise sums over the set of nearest neighbors within a cut-off radius and the slowly converging long-range contribution is solved in reciprocal space. However, this approach remains computationally demanding as the long-range contribution requires several Fourier transforms and the total scheme scales like $\mathcal{O}\left(N_p^{3/2}\right)$ with an optimized cut-off radius [10, 11].

More recently, [12] presented a hybrid approach that calculates the electrostatic forces by calculating separately short- and long range contributions. The former comes from an Eulerian electric field solved using the Poisson equation, while the latter using a truncated pairwise sum along with a correction to avoid double counting. Furthermore, [13] deployed a Fourier-based Ewald summation P^3M method, to accurately capture short- and long-range electrostatic forces that was compared to a classic PM method. It was found that the PM method was capable of quantitatively capturing particle segregation for mono-charged particles. However, it was unable to capture particle chain and ring structures observed using the P^3M method for systems with oppositely charged particles.

In this work, we chose to isolate the inter-particle electrostatic interactions by considering dry mono-charged particles in a vacuum and present how these can be dealt with numerically, especially in case of a tri-periodic computational domain. Next section is dedicated to the numerical method used in this work for computing electrostatic force $\mathbf{F}_e$ for tri-periodic boundary conditions.

2. Numerical calculation of particle-particle electrostatic forces

In this work, particles are considered as mono-disperse, spherical with diameter d_p and inertial, with density ρ_p, thus having a mass $m_p = \rho_p {d_p}^3/6$. Every particle is considered under the point-particle approximation, to bear an equal positive charge Q_p that is concentrated in the particle's center of mass defined as $Q_p = \pi {d_p}^2 \times \rho_Q$, where ρ_Q the particle surface charge density.

Practically, particles are charged via the phenomenon of triboelectrification [14] which occurs when particles collide with walls and other particles. In the simulated periodic particulate flows, it is assumed that particles have had sufficient time to redistribute their charges among them via collisions. However, collisions and triboelectrification are neglected in this study by assuming a very small solid volume fraction. In fact, we consider a theoretical case where the only force acting on the particles is the total electrostatic force $\mathbf{F}_e(\mathbf{x}_p, t)$, so in this case we neglect every other force. This is legitimate in the framework of the objective of this paper, which is to validate a numerical approach for the simulation of these forces. Hence, the particle motion is governed by the following equations of motion

$$\frac{d\mathbf{x}_p}{dt} = \mathbf{u}_p \tag{1}$$

$$m_p \frac{d\mathbf{u}_p}{dt} = \mathbf{F}_e \tag{2}$$

where $\mathbf{u}_p = \mathbf{u}_p(t)$ is the particle velocity at time t. Given initial positions and velocities, a numerical simulation follows all the trajectories by numerical integration. The task at every time-step is to move each particle according to its velocity, and then to update its velocity according to the force exerted by the other particles. Once the total electrostatic force $\mathbf{F}_e$ exerted on a particle is calculated, Eq. (2) is solved in order to update particle velocity and then Eq. (1) to update particle position.

Particle velocities are both time-advanced using an Adams-Bashforth 2nd order scheme coupled with an integrating factor. The numerical solver used in this work is fully parallelized and the particles are distributed over the processors, while at the end of each time-step the latter exchange the particles crossing the CPU borders. Particle positions are initialized using a uniform random distribution and their initial velocities are set to zero, so that they are let to move only due to the potential electric energy stored in the charged particle cloud.

In a system of N_p charged particles, each particle interacts with all $N_p - 1$ particles in the computational domain, thus the total electrostatic force exerted on a particle $\mathbf{F}_e$ is defined as

$$\mathbf{F}_e = \sum_{\substack{q=1 \\ q \neq p}}^{N_p} \mathbf{F}_{q \to p} \tag{3}$$

where $\mathbf{F}_{q \to p}$ is the electrostatic force acting on particle p due to particle q. Coulomb's law allows to calculate the latter as following

$$\mathbf{F}_{q \to p} = \lambda \frac{Q_q Q_p}{\|\mathbf{r}_{pq}\|^3} \mathbf{r}_{pq} \tag{4}$$

where λ is Coulomb's constant with $\lambda = 1/(4\pi\epsilon_0)$ where ϵ_0 is the vacuum permittivity, Q_p is the electric charge of particle p and $\mathbf{r}_{pq} = \mathbf{x}_p - \mathbf{x}_q$ is the distance vector between particles p and q pointing to p as depicted in Fig. 1.

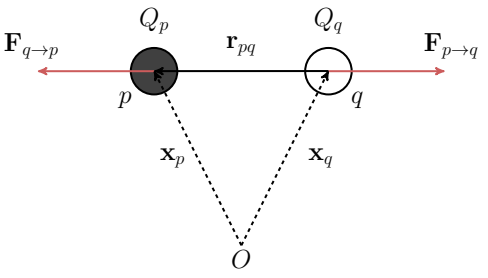

Fig. 1: *Notations in electrostatic interaction of a dipole of mono-charged particles.*

2.1. Electrostatic periodicity

We are interested in an infinite domain, which is usually represented by tri-periodic BCs. We shall see that one of the properties of this infinite domain is a long-range isotropic distribution of the particles. However, before considering periodic BCs, it is important to understand what does this infinity entail physically. Let a spherical domain of radius r that contains mono-charged particles (see Fig. 2). In a

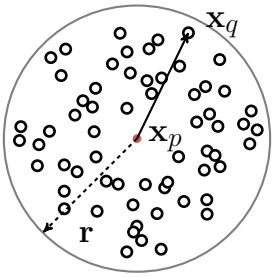

Fig. 2: *Particles in a spherical domain of radius r. Particle of interest (red) lies at position $\mathbf{x}_p$.*

system of N_p charged particles, at every time t, each particle found in position $\mathbf{x}_p$ is immersed in a particle-induced electric field $\mathbf{E}(\mathbf{x}_p, t)$. Therefore, the electrostatic force $\mathbf{F}_e$ exerted on it, is defined as

$$\mathbf{F}_e(\mathbf{x}_p) = Q_p \mathbf{E}(\mathbf{x}_p) \tag{5}$$

$$\mathbf{E}(\mathbf{x}_p) = -\nabla\phi(\mathbf{x}_p) \tag{6}$$

where $\phi(\mathbf{x}_p)$ is the electric potential at position $\mathbf{x}_p$. However, how these two quantities behave for an infinite domain is not trivial. Firstly, for a constant particle number density $n_p = N_p/L^3$, the number of particles that are found inside such a sphere is $N_p(r) = n_p \frac{4}{3}\pi r^3$, thus for an infinite domain it diverges with $N_p(r) \sim r^3$. The electric potential at position $\mathbf{x}_p$ coming from charged particles that are found inside a sphere of radius r is defined as

$$\phi(\mathbf{x}_p \mid r) = \lambda \sum_{q=1}^{N_p(r)} \frac{Q_q}{\|\mathbf{x}_p - \mathbf{x}_q\|} \,. \tag{7}$$

The asymptotic behavior of the electric potential $\phi(\mathbf{x}_p \mid r)$ for an infinite domain can be found theoretically via the following diverging infinite limit

$$\lim_{r\to\infty} \phi(\mathbf{x}_p \mid r) \sim \lim_{r\to\infty} \frac{N_p(r)}{r} \sim \lim_{r\to\infty} r^2 = \infty \tag{8}$$

which means that the electric potential diverges for an infinite domain. However, the electric field at position $\mathbf{x}_p$ coming from charged particles that are found inside a sphere of radius r is defined as

$$\mathbf{E}(\mathbf{x}_p \mid r) = \lambda \sum_{\substack{q=1 \\ \|\mathbf{x}_p - \mathbf{x}_q\| \leq r}}^{N_p(r)} \frac{Q_q}{\|\mathbf{x}_p - \mathbf{x}_q\|^3} (\mathbf{x}_p - \mathbf{x}_q) \ .$$

If now one performs the same asymptotic analysis on the electric field $\mathbf{E}(\mathbf{x}_p \mid r)$, the following infinite limit appears

$$\lim_{r\to\infty} \mathbf{E}(\mathbf{x}_p \mid r) \sim \lim_{r\to\infty} \frac{N_p(r)}{r^3} \sum_{q=1}^{\infty} (\mathbf{x}_p - \mathbf{x}_q) \sim \mathbf{E}_\infty$$

which, in contrast with the limit of Eq. (8), converges towards a spherical infinite sum of vectors $\sum_{q=1}^{\infty} (\mathbf{x}_p - \mathbf{x}_q)$ that due to isotropy converges to a vector $\mathbf{E}_\infty$. This result is important for the calculation of the electrostatic force $\mathbf{F}_e(\mathbf{x}_p)$ for an infinite domain, since it depends linearly on $\mathbf{E}(\mathbf{x}_p)$ as indicated by Eq. (5). Additionally, this result shows the way towards tackling numerically the problem of infinite computations in case of periodic BCs: a decomposition of the total electric field $\mathbf{E}$ into a short-range part that converges to both finite potential ϕ and $\mathbf{E}_\infty$ and into a long-range part whose potential ϕ diverges to infinite but has no contribution on $\mathbf{E}$.

2.1.1. Direct calculation

This simplest and most accurate method for the calculation of inter-particle electrostatic forces consists in calculating the total electrostatic force on each particle by directly summing all the $N_p - 1$ terms that correspond to the electrostatic interactions of a particle with all particles but itself as seen by Eq. (3).

However, one could use Newton's 3rd law for such a dipole that gives $\mathbf{F}_{p\to q} = -\mathbf{F}_{q\to p}$ in order to perform one operation per dipole, thus divide the computational cost by two resulting in $N_p(N_p - 1)/2 \sim {N_p}^2$ operations, which is still forbiddingly expensive. Periodic BCs for the particle phase correspond to an infinite domain. Therefore, to compute the electrostatic forces it is necessary to take into account the contributions of all particles, including those not really represented/computed in the computational domain. Let a cubic computational computational domain Ω of length L as shown in Fig. 3. Consequently, consider a super-domain of (finite) length $(2N_{per} + 1)L$, where N_{per} is the number of domain images per direction i.e. the number of periodic layers around the domain (see Fig. 4). If d is the number of (periodic) physical dimensions, then the total number of periodic domain images including the original one is $(2N_{per} + 1)^d$. In theory, periodic BCs are exactly represented for $N_{per} \to \infty$, however in practice N_{per} will be considered finite based on a convergence criterion which entails a cut-off error (see Fig. 7), hence these BCs are considered as quasi-periodic.

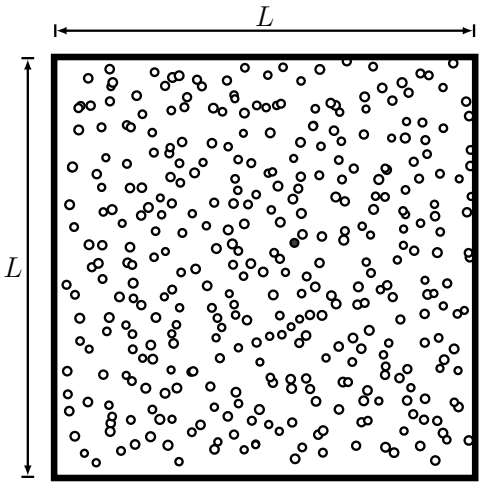

Fig. 3: *Computational domain of interest Ω of length L containing N_p particles. A particle (black-filled circle) interacts electrostatically with all $N_p - 1$ other particles in the domain.*

Apparently, since the computational domain (and its periodic images) is cubic, the periodic super-domain is also cubic. For the sake of simplicity but without violating generality, if we reason per direction, this implies that for a finite number of periodic layers N_{per}, any particle, that is not found exactly in the center of the computational domain (center of symmetry in this case), interacts roughly with N_{per} periodic domain images towards the closest border, while with $N_{per}+1$ images towards the opposite direction (N_{per} periodic layers + the computational domain). This becomes intuitively evident, if we take a particle that is in the corner of the computational domain as shown in Fig. 4. Evidently, for $N_{per} \to \infty$ the ratio $(N_{per}+1)/N_{per} \to 1$ but for N_{per} finite, this convergence is very slow as seen in Table 1.

Table 1: *Slow convergence of periodic anisotropy*

N_{per}	1	2	3	4	5	6	7	8	9	10
$\frac{N_{per}+1}{N_{per}}$	2.00	1.50	1.33	1.25	1.20	1.17	1.14	1.12	1.11	1.10

In fact, any particle with an offset from the domain center (essentially all particles) would always interact with less particles located to the direction of that offset than the opposite direction. Consequently, it would be subjected to a force that always points outwards of the domain (towards the closest border) that would be proportional to the offset in question, which implies an anisotropic distribution of long-range electrostatic forces. As a result, most particles would accelerate towards the domain borders and due to periodicity re-enter from the opposite side where they would re-accelerate outwards, which would eventually result in an oscillation of the particles across the borders. This behavior is not physical and in order to avoid it, each particle should interact only with the particles (real and images) that are located within a periodic cubic volume that is centered at the particle position $\mathbf{x}_p$ (see Fig. 4) and has an edge $\alpha_c = (2N_{per} - 1)\, L$. In this way, the isotropy of the long-range electrostatic force distribution is ensured as the particle in question lies

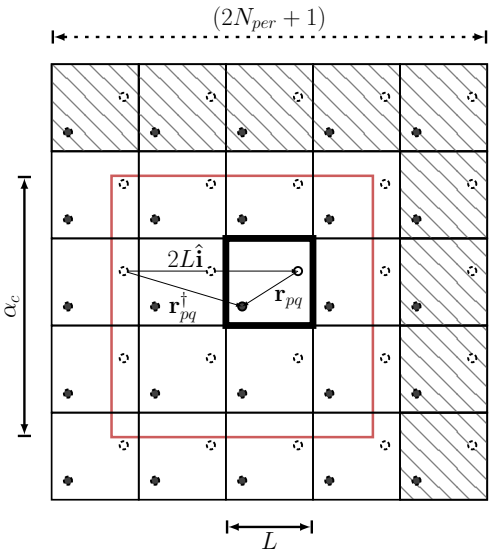

Fig. 4: *Quasi-periodic BCs with N_{per} periodic layers. The computational domain Ω is marked with bold contours, while its periodic images with thin ones. Two particles are put in the domain for simplicity and for each one, a periodic cubic volume (red contour) of edge $\alpha_c = (2N_{per}-1)\,L$ is centered at its respective position, intersecting only $2N_{per}$ periodic domain images per direction, hatched ones ignored for p).*

in the center of a periodic cubic volume that by definition extends to $(\mathbf{x}_p \pm \alpha_c/2)$. Hence, for tri-periodic BCs the periodic cubic volume includes exactly $(2N_{per}-1)^3$ periodic domain images, thus $(2N_{per}-1)^3 N_p$ particles (real and images). As a result, $\mathbf{F}_{q\to p}$ is the sum of all $(2N_{per}-1)^3 - 1$ interactions due to particle q and its periodic images as

$$\mathbf{F}_{q\to p} = \lambda Q_q Q_p \sum_{\substack{l,m,n=-N_{per}^{N_{per}} \\ |r^{\dagger}_{pq,i}|\leq\alpha_c}} \frac{\mathbf{r}^{\dagger}_{pq}}{\left\|\mathbf{r}^{\dagger}_{pq}\right\|^3} \,. \tag{9}$$

where $\mathbf{r}^{\dagger}_{pq}$ is the periodic particle distance vector that can be simply calculated as a translation of the original distance vector as $\mathbf{r}^{\dagger}_{pq} = \mathbf{r}_{pq} + \mathbf{n}L$, where $\mathbf{n} = m\hat{\mathbf{i}} + n\hat{\mathbf{j}} + l\hat{\mathbf{k}}$ is a translation vector for the periodic domain image with indices $l, m, n = -N_{per}, N_{per}$ and $\hat{\mathbf{i}}$, $\hat{\mathbf{j}}$, $\hat{\mathbf{k}}$ denote the Cartesian unit vectors. In addition, the periodic volume intersects only with $2N_{per}$ periodic domain images per direction, an a priori knowledge that allows for a small computational gain in terms of operations when computing periodic $\mathbf{F}_{q\to p}$ from Eq. (9). However, any computational gain becomes important when the number of particles and time-steps is really large due to accumulation effect. Hence, in case of tri-periodic BCs, to calculate the total electrostatic force exerted on a particle $\mathbf{F}_e$, one should estimate the sum of Eq. (3) over $(2N_{per}-1)^3 (N_p - 1)$ real and image particles in the periodic cubic volume. In practice, if the positions of N_p particles in the domain Ω are known, then for the calculation of $\mathbf{F}_e$ only $N_p - 1$ distance vectors $\mathbf{r}_{pq}$ are needed for the rest $(2N_{per}-1)^3 (N_p - 1)$ particles in Ω and their images. For periodic BCs, the computational cost of the direct method, $\mathcal{C}$ can be written, in terms of number of summations, as $\mathcal{C}(N_p, N_{per}) = (2N_{per}-1)^3 N_p (N_p - 1)/2 \sim 4{N_{per}}^3 {N_p}^2$.

2.1.2. Isotropy of the periodic (long-range) electrostatic forces

As explained earlier, it is very important, for the correct representation of the simulated physics in an infinite domain with a homogeneous isotropic statistical distribution of particles, that the quasi-periodic BCs are applied in such a way that the isotropy of the long-range electrostatic forces is ensured. To this end, one can calculate high order statistical moments of fluctuations of the electrostatic force $\mathbf{F}'_e = \mathbf{F}'_e - \langle \mathbf{F}_e \rangle_p$, where $\langle \, . \, \rangle_p$ is the average operator over the particles in the computational domain.

Since $\mathbf{F}_e$ is a vector field known at the particle positions, one can calculate Lagrangian tensor $\langle F'_{e_i} F'_{e_j} \rangle_p$, which is a measure of the corresponding electric field (see Subsect. 3.4) and contains 9 components

$$\langle F'_{e_i} F'_{e_j} \rangle_p = \begin{bmatrix} \langle {F'_{e_x}}^2 \rangle_p & \langle F'_{e_x} F'_{e_y} \rangle_p & \langle F'_{e_x} F'_{e_z} \rangle_p \\ \langle F'_{e_y} F'_{e_x} \rangle_p & \langle {F'_{e_y}}^2 \rangle_p & \langle F'_{e_y} F'_{e_z} \rangle_p \\ \langle F'_{e_z} F'_{e_x} \rangle_p & \langle F'_{e_z} F'_{e_y} \rangle_p & \langle {F'_{e_z}}^2 \rangle_p \end{bmatrix} \tag{10}$$

whose intensity can be defined as $F^2 = \left(\langle {F'_{e_x}}^2 \rangle_p + \langle {F'_{e_y}}^2 \rangle_p + \langle {F'_{e_z}}^2 \rangle_p \right) / 3$. To verify the property of isotropy of tensor defined in Eq. (10), a case study has been considered with $N_p = 10,000$ particles of density $\rho_p = 2,750 \ kg/m^3$ in a domain of size $L = 2\pi \ m$ bearing an electric charge $Q_p = 5 \times 10^{-9} C$ and using $N_{per} = 1$ periodicity layers.

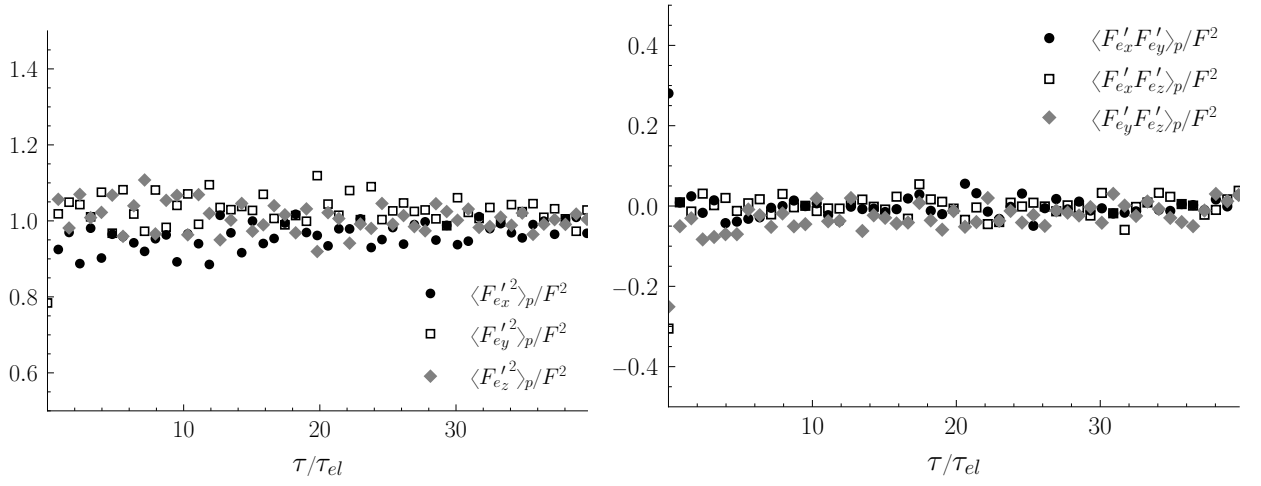

(a) *Diagonal elements.* **(b)** *Off-diagonal elements.*

Fig. 5: *Time evolution of Lagrangian tensor of electrostatic forces* $\langle F'_{e_i} F'_{e_j} \rangle_p$.

The time evolution of the diagonal and off-diagonal components of the Lagrangian electrostatic forces tensor $\langle F'_{e_i} F'_{e_j} \rangle_p$ is presented in Fig. 5. These plots have included the transition phase, as particles start at $t = 0$ accelerating from zero initial velocities having a uniform random distribution due to the stored electric potential energy. This means that at the beginning of the particle motion, the electric field of the particles (which is a non-linear function of their positions) constitutes an anisotropic solution of the system, as at $t = 0$ it does not respect the minimal energy principle of the conservative electrostatic forces.

However, once set in motion, the system tends to minimize its electric potential energy, and the developed

method ensures the isotropy of the electric field, in the stationary regime. This means that, in order to acquire a more statistically converged average of these terms, if we take a time average of the aforementioned terms after the 10s mark, when we enter a stationary regime, we get

$$\langle {F_{e_x}'}^2 \rangle = \langle {F_{e_y}'}^2 \rangle = \langle {F_{e_z}'}^2 \rangle = F^2$$
$$\langle F_{e_i}' F_{e_j}' \rangle = 0, \ \forall i,j = x,y,z, \ i \neq j \ .$$

which affirms the isotropy of the electric field.

2.1.3. Convergence of the periodic (long-range) electrostatic forces

Theoretically, as shown in Subsect. 2.1, from the point of view of a particle in the periodic volume, as more particle images are taken into account around it, there is a cut-off distance after which the total long-range electrostatic forces that are exerted on it tend to cancel out as $N_{per} \to \infty$.

However, since in a computational framework N_{per} has to be finite, the inevitable question rises: how many periodic layers N_{per} are needed to achieve convergence of the quasi-periodic electrostatic force calculation? As more periodic domain images are taken into consideration, a particle that lies in the computational domain interacts with more particles $\propto {N_{per}}^3$ that are placed in an increasingly greater distance $\left\|\mathbf{r}_{pq}^{\dagger}\right\| \propto N_{per}$. The electric potential energy stored in a particle, u_e is defined as

$$u_e\left(\mathbf{x}_p\right) = Q_p \phi\left(\mathbf{x}_p\right) \tag{11}$$

which, can be calculated Lagrangianly as

$$u_e\left(\mathbf{x}_p\right) = \lambda Q_p \sum_{\substack{q=1 \\ q \neq p}}^{N_p} Q_q \sum_{\substack{l,m,n=-N_{per} \\ \left|r_{pq,i}^{\dagger}\right| \leq \alpha_c}}^{N_{per}} \frac{1}{\left\|\mathbf{r}_{pq}^{\dagger}\right\|} \propto {N_{per}}^2 \tag{12}$$

which implies that the particle electric potential energy diverges quadratically for tri-periodic BCs as shown by Fig. 6 (left). As far as the total electrostatic force on a particle is concerned, the same behavior is in place due to periodicity, however it should be noted that $\|\mathbf{F}_e\| \propto 1/\left\|\mathbf{r}_{pq}^{\dagger}\right\|^2 \propto 1/{N_{per}}^2$. From Eq. (3), one can deduce that

$$\mathbf{F}_e = \lambda Q_p \sum_{\substack{q=1 \\ q \neq p}}^{N_p} Q_q \sum_{\substack{l,m,n=-N_{per} \\ \left|r_{pq,i}^{\dagger}\right| \leq \alpha_c}}^{N_{per}} \frac{\widehat{\mathbf{r}}_{pq}^{\dagger}}{\left\|\mathbf{r}_{pq}^{\dagger}\right\|^2} \propto \sum_{\substack{m=-N_{per} \\ \left|r_{pq,i}^{\dagger}\right| \leq \alpha_c}}^{N_{per}} \widehat{\mathbf{f}}_e^{(m)} = \mathbf{f}_e. \tag{13}$$

In fact, Fig. 6 (right) shows that electrostatic forces converge very quickly for $N_{per} \geq 2$. This convergence is sufficient to correctly simulate periodic particle-particle electrostatic interactions, albeit the divergence of the electric potential energy, as $\mathbf{F}_e$ drives particle motion (see Eq. (2)).

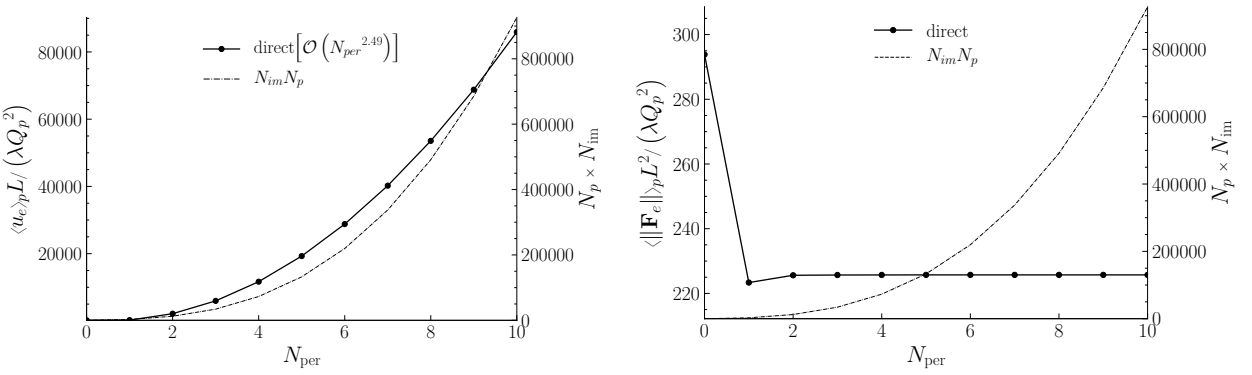

Fig. 6: *Average particle electric potential energy (left) and average norm of the electrostatic force (right) with regard to the number of periodic domain images for $N_p = 100$. Quadratic divergence is observed for the former, while convergence for the latter at $N_{per} \geq 2$. The total number of particles with their periodic images is $N_p \times N_{im}$ where N_{im} is the number of domain images (see Sect. Appendix A.2).*

Admittedly, the choice of a finite N_{per} entails a cut-off error. To estimate it, simulations have been performed with the same distribution of N_p particles for an increasing number of periodic layers N_{per}. Considering the simulation with the maximum number of periodic layers $N_{per}^{\max}$ as the simulation of highest

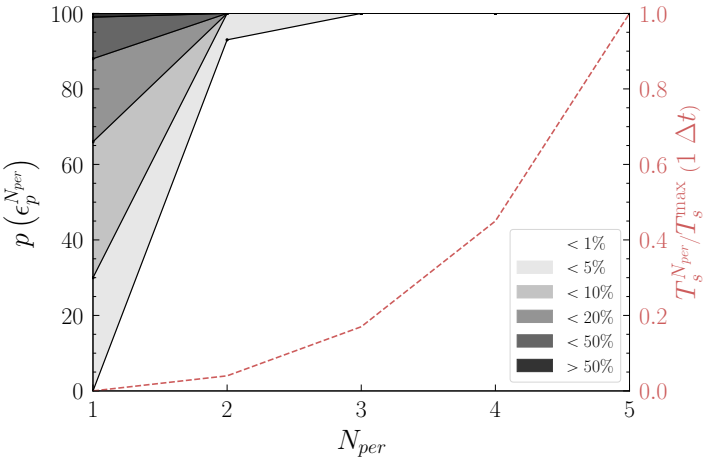

Fig. 7: *Relative cut-off error distribution of the electrostatic forces exerted on the particles for one time-step with regard to number of periodic layers N_{per} for direct algorithm with $N_p = 100$. Reference simulation is conducted with $N_{per} = 5$. A different shade of grey is attributed to the percentage of particles for which the cut-off error is between 0%, 1%, 5%, 10%, 20% and 50%. The red dashed line is the cost of simulation. Sufficient convergence is observed for $N_{per} \geq 2$.*

fidelity, the relative error of the total electrostatic force for each particle p at $t = t_0$, $\epsilon_p^{N_{per}}(\mathbf{x}_p, t_0)$ has been calculated for each number of periodic layers N_{per} as

$$\epsilon_p^{N_{per}}(\mathbf{x}_p, t_0) = \frac{\left\| \mathbf{F}_e^{N_{per}}(\mathbf{x}_p, t_0)\Big|_{\text{direct}} - \mathbf{F}_e^{N_{per}^{\max}}(\mathbf{x}_p, t_0)\Big|_{\text{direct}} \right\|}{\left\| \mathbf{F}_e^{N_{per}^{\max}}(\mathbf{x}_p, t_0)\Big|_{\text{direct}} \right\|} .$$

The left vertical axis of Fig. 7 shows the percentage of particles, $p\left(\epsilon_p^{N_{per}}\right) = N_p \Big|_{\epsilon_{\min}^{N_{per}} \leq \epsilon_p^{N_{per}} \leq \epsilon_{\max}^{N_{per}}} / N_p$

for which the cut-off error $\epsilon_p^{N_{per}}$ is bounded between $\epsilon_{\min}^{N_{per}}$ and $\epsilon_{\max}^{N_{per}}$. A fast convergence is achieved for $N_{per} \geq 2$, while for $N_{per} \geq 3$ absolute convergence is observed. However, the cut-off error for $N_{per} = 1$, albeit considerable, seems to be less than 20% for approximately 90% of the particles in the computational domain. A way to understand the effect of the long-range field of electrostatic forces is to calculate the total electrostatic force that is exerted on a particle coming from particles that are found in an increasing distance that is defined as

$$\mathbf{F}_e(r) = \sum_{\substack{q=1, q\neq p \\ -\Delta r/2 \leq \|\mathbf{r}_{pq}\| - r \leq \Delta r/2}}^{N_p} \mathbf{F}_{q\to p}\left(\mathbf{r}_{pq}\right) \ .$$

Figure 8 shows that the contribution of the long-range part of electrostatic forces becomes negligible after a specific distance. The fact that this distance is smaller than half the size of the computational domain is what allows to correctly assume periodic boundary conditions in this system of charged particles, as well as justifies the choice of $N_{per} = 1$, albeit the local cut-off error.

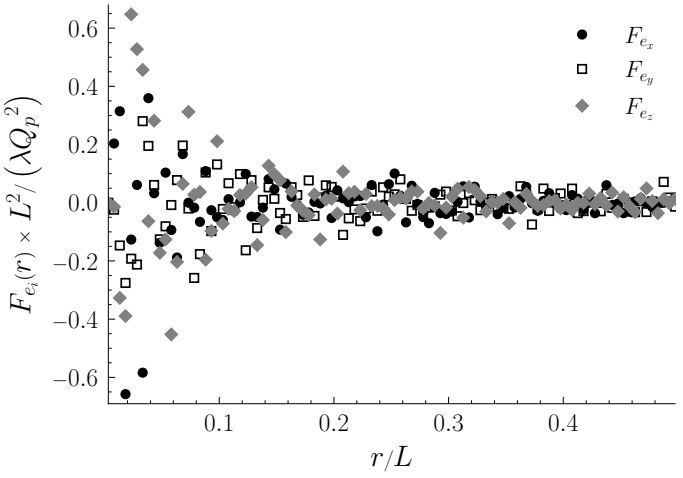

Fig. 8: *Total electrostatic force exerted on a particle due to interaction with particles that are found within an annular shell of between radius* $r \pm \Delta r/2$ *with* $\Delta r = L/100$.

Furthermore, Fig. 9 shows the time evolution of the particle agitation (particle kinetic energy per unit mass) $q_p^2 = 1/2\langle u'_{p,i} u'_{p,i}\rangle_p$ and the mean electrostatic force per unit mass $\langle\|\mathbf{F}_e\|\rangle_p/m_p$ in the transient and stationary regime. The observed attenuated oscillatory behavior is examined in Subsect. 3.4. It seems that the cut-off error for $N_{per} = 1$ affects mostly the transition to the statistically steady regime but not the statistical average after stationarity is reached.

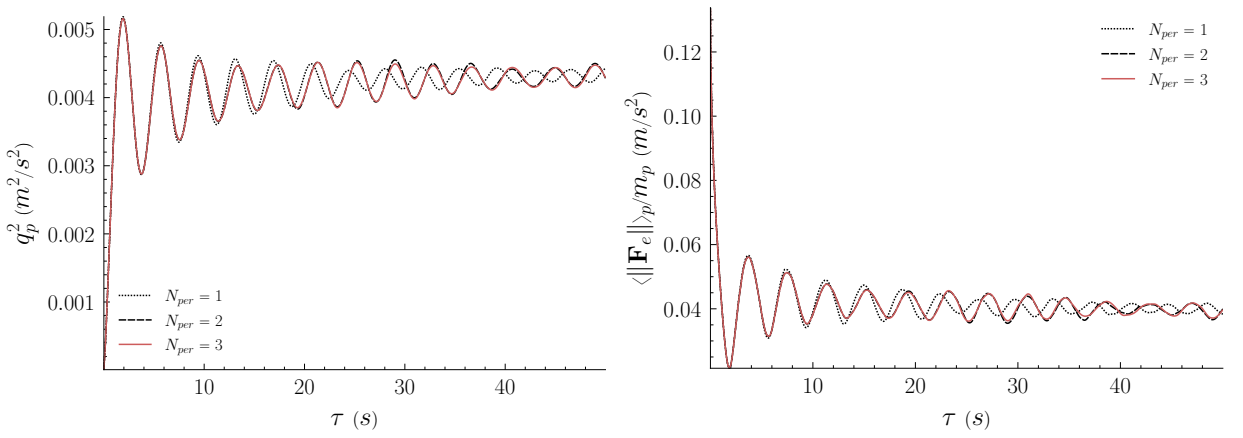

Fig. 9: *Evolution of particle agitation and mean electrostatic acceleration for increasing number of periodic layers N_{per}. Convergence of statistics for the stationary regime is observed for $N_{per} \geq 1$.*

Therefore, it can be considered negligible for a 1st order approximation, as it only affects higher-order dynamics of the particulate flow, a conclusion that is in agreement with the conclusions of [15]. Thus, it seems reasonable for the simulations carried out in this work, to choose $N_{per} = 1$. This way, the domain is replicated only one time towards each direction, which means that each particle of the computational domain is centered in a cubic periodic volume of length L in which it interacts with $N_p - 1$ particles. This choice of N_{per} enables calculations of a large number of particles $10^4 \leq N_p \leq 10^6$ within reasonable computational time and acceptable statistical error.

2.2. Pseudo-particle method

Let the computational domain Ω be discretized in N_e cells per direction (see Fig. 10) of length $\Delta x_f = L/N_e$, so that each cell Ω_k contains $N_k = \sum_{n=1}^{N_p} \delta_k^{(n)} \sim N_p/{N_e}^3$ particles. Evidently, it is reasonable that $N_k \gg 1$ which leads to a maximum number of cells $N_e^{\max}$ defined as $N_e^{\max} = {N_p}^{1/3}$. Each Ω_k forms a pseudo-particle, which is a cluster of particles "viewed" from distance as one particle of equivalent charge Q_k^{eq} and position $\mathbf{x}_k^{eq}$. The concept of pseudo-particles, inspired by [3], is defined in Eq. (14)-(16) and is illustrated in Fig. 10.

$$Q_k^{eq} = \sum_{p=1}^{N_p} \delta_{pk} Q_p \tag{14}$$

$$\mathbf{x}_k^{eq} = \frac{1}{Q_k^{eq}} \sum_{p=1}^{N_p} \delta_{pk} Q_p \mathbf{x}_p \tag{15}$$

where $\delta_{pk} = \delta\left(\mathbf{x}_p - \mathbf{x}_k^c\right)$ is the indicator function defined as

$$\delta_{pk} = \begin{cases} 1, & \text{if } \mathbf{x}_p \in \Omega_k \\ 0, & \text{otherwise} \end{cases} \tag{16}$$

and $\mathbf{x}_k^c$ is the center of pseudo-particle cell Ω_k.

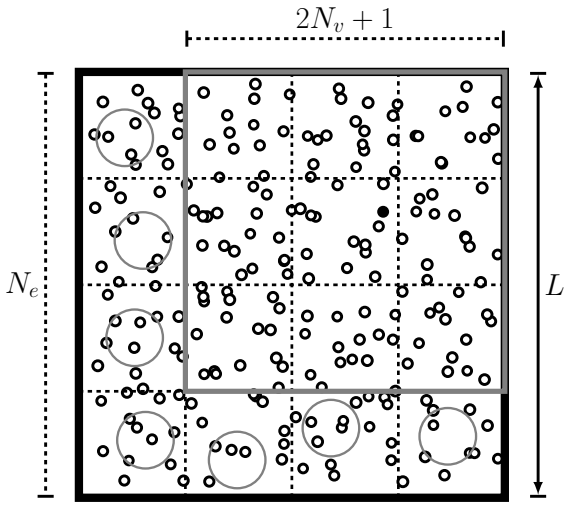

Fig. 10: *Computational domain Ω of length L is discretized in N_e cells per direction. For each particle p (black-filled circle), its neighborhood V_p (bold gray) spans $2N_v + 1$ cells to each direction. Pseudo-particles (gray circles) are defined for every cell Ω_k outside of V_p.*

For each particle n, its neighborhood $V_p^{(n)}$ of size $\Delta x_v = (2N_v + 1)\,\Delta x_f$ is defined as the ensemble of $(2N_v + 1)^3$ cells around it. N_v is the number of cells for which the neighborhood spans towards every direction x, y, z (excluding the cell that contains the particle), i.e. the number of layers of direct computation around the cell of a particle. Therefore, each particle interacts directly with all particles in neighborhood V_p (short-range interaction), as well as with the pseudo-particles that are outside of V_p (long-range interaction). This allows to accurately calculate the short-range part of $\mathbf{F}_e$, which contains most of the information, while committing an acceptable approximation error for the long-range part. It should be noted that the total approximation error introduced from such a decoupling, depends both on the number of cells, N_e but also on the number of neighbourhood cells, N_v.

Observing Fig. 10, it is evident that for $N_v = 0$ the particle neighbourhood is limited to the very cell to which it belongs. This implies that particles close to the borders of its cell, would interact in proximity with the pseudo-particle of the adjacent cell which would be a violation of the very concept of pseudo-particles. For this reason, the pseudo-particle algorithm can provide reasonable results only for $N_v > 0$ (see Fig. 16). The electrostatic force $\mathbf{F}_{k\to p}$ acting on particle p due to pseudo-particle Ω_k is calculated by treating Ω_k as another particle, meaning that Q_q is replaced by Q_k^{eq} and $\mathbf{x}_q$ by $\mathbf{x}_k^{eq}$ in Eq. (4). Hence, the total electrostatic force on particle p is calculated by performing direct and pseudo-particle summations inside and outside of V_p, respectively. Therefore, the total electrostatic force exerted on a particle is calculated as

$$\mathbf{F}_e = \underbrace{\sum_{\substack{k=1 \\ k\in V_p}}^{{N_e}^3} \sum_{\substack{q=1 \\ q\neq p}}^{N_k} \mathbf{F}_{q\to p}}_{\substack{\text{short-range} \\ (2N_v+1)^3 N_p/{N_e}^3 - 1 \text{ terms}}} + \underbrace{\sum_{\substack{k=1 \\ k\notin V_p}}^{{N_e}^3} \mathbf{F}_{k\to p}}_{\substack{\text{long-range} \\ {N_e}^3 - (2N_v+1)^3 \text{ terms}}} . \tag{17}$$

The presented pseudo-particle method (Eq. (14)-(16)) only accounts for the first moment of the particle

distribution (the center of charge) and thus relies on an assumption of equally distributed particles of equal charge. In the case where these assumptions are invalid, the error of this simplification could be of significant size. Although this is a disadvantage of the presented method, it does not alter the presented solution for quasi-periodic BCs and its implementation (see Subsect. 2.2.1), which could be applied to any hierarchical method. Using either a multipole-method or a particle-mesh interpolation could be a solution to this.

2.2.1. Quasi-periodic boundary conditions

First of all, the following analysis is based on conclusions deduced in Subsect. 2.1 concerning the periodic BCs (isotropy and convergence of long-range interactions). Let the computational domain Ω be discretized in N_e cells per direction. Evidently, the direct neighbourhood V_p that spans $2N_v + 1$ cells should fit inside the periodic cubic volume that spans $(2N_{per} - 1)\, N_e$ cells (as shown by Fig. 11), thus N_v and N_e must satisfy the inequality

$$2N_v + 1 \leq (2N_{per} - 1)\, N_e - 1 \ . \tag{18}$$

As explained in Subsect. 2.1, the super-domain needed to impose periodic BCs for each particle is of length $2N_{per}L$, inside of which the periodic cubic volume of length $\alpha_c = (2N_{per} - 1)\, L$ is defined as shown in Fig. 11. The electrostatic force acting on a particle p due to a pseudo-particle Ω_k, $\mathbf{F}_{k\to p}$ is the sum of $(2N_{per} - 1)^3$ interactions due to Ω_k and its periodic images as

$$\mathbf{F}_{k\to p} = \lambda Q_k^{eq} Q_p \sum_{\substack{l,m,n=-N_{per} \\ |r^{\dagger}_{kp,i}| \leq \alpha_c}}^{N_{per}} \frac{\mathbf{r}^{\dagger}_{kp}}{\left\| \mathbf{r}^{\dagger}_{kp} \right\|^3} \tag{19}$$

where $\mathbf{r}_{kp} = \mathbf{x}_p - \mathbf{x}_k^{eq}$ is the distance vector between particle p and pseudo-particle Ω_k.

However, the notion of periodic cubic volume centered on each particle in combination with the pseudo-particles defined in each cell, introduces a subtle complexity regarding the treatment in the borders of the periodic cubic volume in question. In Fig. 11 one can observe that inevitably the borders of the periodic cubic volume will intersect specific cells (for each particle). Since each pseudo-particle Ω_k has an associated equivalent position $\mathbf{x}_k^{eq}$ and charge Q_k^{eq}, a simple solution could be to include pseudo-particles that lie inside the periodic cubic volume based on their position $\mathbf{x}_k^{eq}$.

In fact, each pseudo-particle represents a large number of particles N_k, thus a significant contribution in $\mathbf{F}_e$. As a result, considering a uniform distribution of particles, every particle that has a significant offset from its cell center would be subjected to an electrostatic force that always points outwards of the domain (towards the closest border) that would be proportional to the offset in question, which implies an anisotropic long-range electrostatic force distribution. As a result, most particles would accelerate towards the cell borders and ultimately present a non physical behavior similar to that caused by an anisotropic application of the periodic BCs explained in Subsect. 2.2.1 this time on the level of the cells.

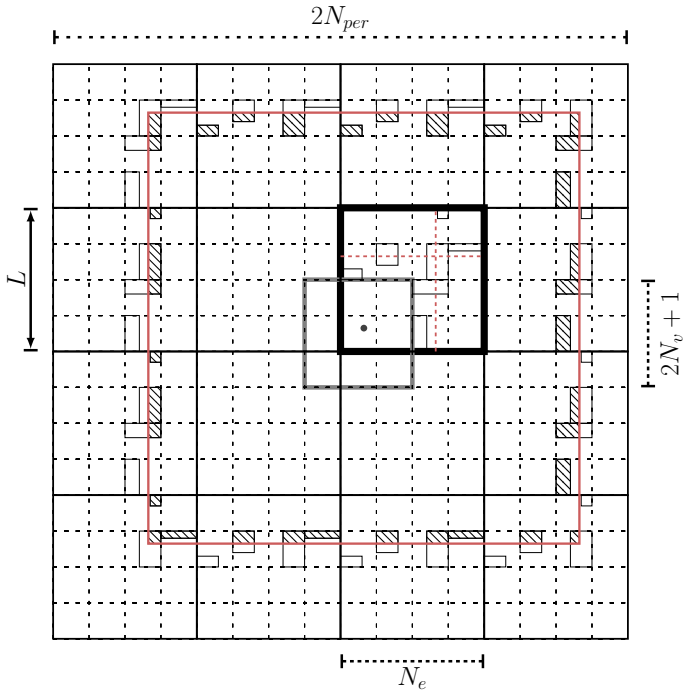

Fig. 11: *Domain of interest Ω (bold black) of length L, periodic domain images (thin black) with $N_{per} = 2$ and periodic cubic volume (red) of edge $\alpha_c = 3L$. Neighborhood V_p (gray) with $N_v = 1$ spans over several images of Ω. Every pseudo-particle cell Ω_k can be represented by a rectangle of equivalent charge density $\rho^{eq}_{q,k}$ centered at $\mathbf{x}^k_{eq}$ that extends up to the closest cell borders. Thus, a cell that is intersected by the periodic volume borders at position $\mathbf{x}_c$ can be represented by a section of the corresponding rectangle (hatched).*

To ensure the isotropy of the long-range electrostatic interactions on the cell level, it is imperative that a smarter treatment should be put in place for the border cells of the periodic volume. Based on the work of [15], each pseudo-particle Ω_k can be represented as a rectangular charged cloud of particles X_k of total equivalent electric charge Q^{eq}_k that is centered at $\mathbf{x}^{eq}_k$ and extends up to the closest cell borders. That means that this pseudo-particle rectangle, has an equivalent (constant) charge density $\rho^{eq}_{q,k}$ defined as

$$\rho^{eq}_{q,k} = \frac{Q^{eq}_k}{\Delta x_k \Delta y_k \Delta z_k}$$

where $\Delta \mathbf{x}_k$ are the dimensions of pseudo-particle rectangle X_k (see Sect. Appendix A.1). Evidently, for each particle the intersected cells can be easily found as the periodic volume intersects a periodic domain image at position $\mathbf{x}_c$, whose components can be calculated as $x_{c,i} = (x_{p,i} + \alpha_c) \bmod L$. Once the intersected pseudo-particle cells are identified, the correct section of the corresponding pseudo-particle rectangle has to be taken into account which depends on each translation to account for periodicity. Finally, using Eq. (19) for $\mathbf{F}_{k \to p}$ in Eq. (17), with the appropriate corrections for border cells, the total electrostatic force exerted on a particle can be calculated using the pseudo-particle method and quasi-periodic BCs.

2.2.2. Computational cost and performance

Therefore, for each particle in Ω we take into consideration $\sim (2N_v+1)^3 N_p/{N_e}^3$ direct interactions and $(2N_{per}-1)^3 {N_e}^3$ pseudo-particle interactions, considering the cost of pseudo-particle intersections negligible. As a result, the computational cost with periodic BCs becomes

$$\mathcal{C}(N_p, N_e, N_v, N_{per}) = N_p \left[\underbrace{(2N_v+1)^3 N_p/{N_e}^3 - 1}_{\text{short-range}} + \underbrace{(2N_{per}-1)^3 {N_e}^3 - (2N_v+1)^3}_{\text{periodic long-range}} \right] \tag{20}$$

where it is evident that the computational cost of the (costly) short-range part is proportional to the number of particles N_p and the number of cells in the neighbourhood $\sim {N_v}^3$, while it is inversely proportional to the number of cells ${N_e}^3$. However, the (smaller) long-range part is proportional ${N_e}^3$. Therefore, the dependence of $\mathcal{C}(N_p, N_e, N_v, N_{per})$ on N_e is not evident. Figure 12 shows that if $N_v = \text{cst}$, as N_e increases it is evident that for $N_e \sim {N_p}^{\frac{1}{3}} \Rightarrow N_k \sim 1$ each cell Ω_k would contain at most one particle, hence the method would degrade to the direct method in terms of performance.

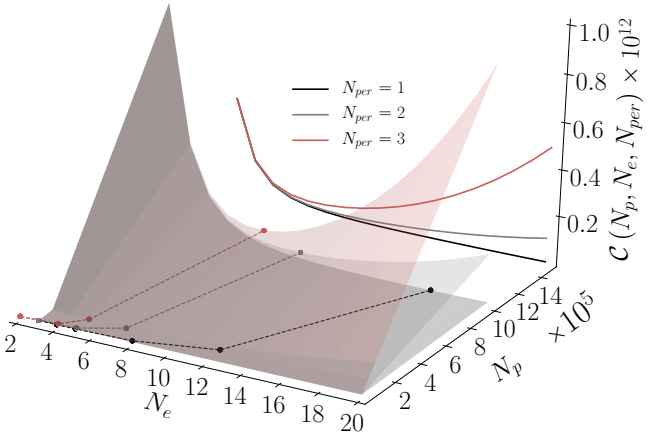

Fig. 12: *Theoretical computational cost of periodic pseudo-particle method for $N_v = 1$.*

On the other hand, for smaller values of N_e, each cell would contain a large number of particles N_k, which means that a large portion of the electrostatic force calculations would be performed inside the neighbourhood as the size of each cell Δx_f would be relatively large, thus the neighbourhood size Δx_v would also be large. This means that for every number of particles N_p, there is an optimal number of cells $N_e^{opt} \in [(2N_v+2)/(2N_{per}-1), {N_p}^{1/3}]$ that minimizes the function of the computational cost of Eq. (20) (see Sect. Appendix A.2). In this case the optimal computational cost would be

$$\mathcal{C}^{opt}(N_p, N_v, N_{per}) = N_p \left[2\sqrt{N_p (2N_{per}-1)^3 (2N_v+1)^3} - (2N_v+1)^3 - 1 \right] \sim {N_p}^{\frac{3}{2}} {N_v}^{\frac{3}{2}} {N_{per}}^{\frac{3}{2}} .$$

Figure 13 shows that the calculated order of complexity $\sim {N_p}^{1.5}$ is of similar order of magnitude than the expected theoretical one. The performance of the algorithm has been calculated for an optimal number of cells N_e^{opt} for every level of particle number N_p, as the algorithm has merit only for such a configuration.

In addition, the observed slight overestimation of the anticipated theoretical value comes from the special treatment of the borders of the cubic volume in order to account for periodic BCs.

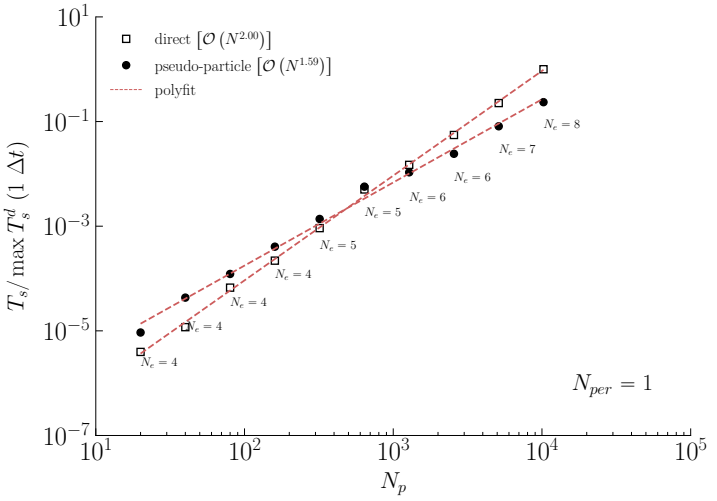

Fig. 13: *The simulation time (1 Δt) for direct and pseudo-particle algorithm ($N_v = 1$ and $N_{per} = 1$) normalized by its maximum value (for direct algorithm) is plotted against an increasing number of particles for optimal number of cells N_e^{opt}.*

2.2.3. Approximation error analysis

The direct method is considered to be of high fidelity as it allows for an exact calculation of the electrostatic forces, except for the cut-off error due to quasi-periodic BCs. Hence the results obtained with this method constitute a reference for simulations using an approximative method such as the pseudo-particle method. Therefore, the relative error of total electrostatic force estimation for particle p at $t = t_0$, $\epsilon_p^{N_e}(\mathbf{x}_p, t_0)$ has been calculated for each number of cells per direction N_e as

$$\epsilon_p^{N_e}(\mathbf{x}_p, t_0) = \frac{\left\| \mathbf{F}_e^{N_e}(\mathbf{x}_p, t_0)\Big|_{\text{pseudo}} - \mathbf{F}_e^{N_{per}}(\mathbf{x}_p, t_0)\Big|_{\text{direct}} \right\|}{\left\| \mathbf{F}_e^{N_{per}}(\mathbf{x}_p, t_0)\Big|_{\text{direct}} \right\|} .$$

The left vertical axis of Fig. 14 shows the percentage of particles, $p\left(\epsilon_p^{N_e}\right) = N_p \Big|_{\epsilon_{\min}^{N_e} \le \epsilon_p^{N_e} \le \epsilon_{\max}^{N_e}} / N_p$ for which the approximation error $\epsilon_p^{N_e}$ is bounded between $\epsilon_{\min}^{N_e}$ and $\epsilon_{\max}^{N_e}$. The committed error is quasi-constant for $N_e < 10$ and then it decreases considerably for $N_e \geq 10$. For small values of N_e each pseudo-particle would contain a large number of particles $N_p/{N_e}^3$, thus it would be a crude approximation of the cluster of particles that it represents. However, at the same time the size of each cell Δx_f would be relatively large, hence every such interaction would occur far away from the particle of interest at a distance $\geq \Delta x_v$. Therefore, the errors observed are rather moderate as only $\sim 10\%$ of particles have an error $20\% < \epsilon_p^{N_e} < 50\%$. Increasing the number of cells N_e reduces the number of particles per cell $N_k = N_p/{N_e}^3$. However, at the limit of $N_k \sim 1$, where some cells contain at most one particle while some are empty, some of them will be cut by the periodic volume resulting in a rather crude approximation of one particle via sections of the corresponding

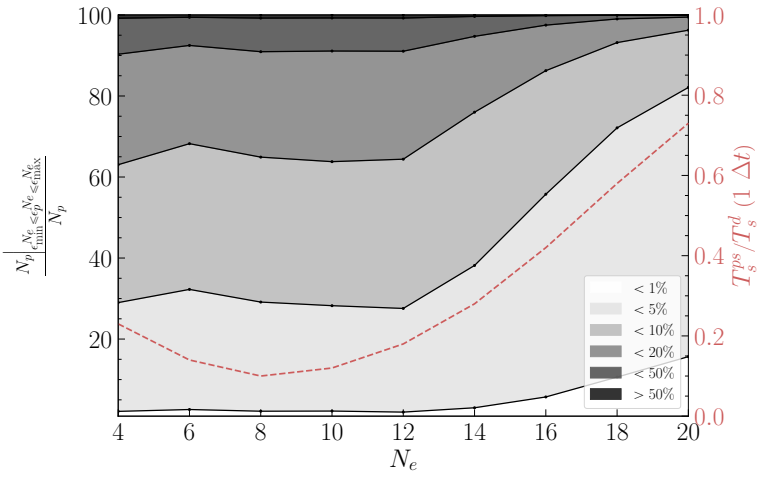

Fig. 14: *Relative approximation error distribution with regard to number of cells N_e of pseudo-particle algorithm for one time-step and $N_p = 10,000$. A different shade of gray is attributed to the percentage of particles for which the approximation error is between 0%, 1%, 5%, 10%, 20% and 50%. The red dashed line shows the simulation time of the pseudo-particle algorithm ($N_v = 1$, $N_{per} = 1$) normalized by that of the direct algorithm for the same case.*

pseudo-particle rectangle which entails a remaining error that is hard to eliminate.

2.3. Verification of the numerical methods

To verify the direct method, one can use Newton's 3rd law that for a $p - q$ electric dipole states that the electrostatic force exerted on a particle p due to particle q is opposite of the force exerted on particle q due to particle q, or $\mathbf{F}_{p\to q} = -\mathbf{F}_{q\to p}$. For direct algorithm and quasi-periodic boundary conditions, every particle in the computational domain interacts with $(2N_{per} - 1)^3 N_p$ particles (real and images). Therefore, theoretically the average of electrostatic forces exerted on all N_p particles of the computational domain should be zero, or $\langle F_{e_i}\rangle_p = 0$, hence this can be used as a verification criterion. In order to examine that, the time evolution of the Lagrangian average of all three components of particle electrostatic forces $\langle F_{e_x}\rangle_p$, $\langle F_{e_y}\rangle_p$, $\langle F_{e_z}\rangle_p$ are plotted in Fig. 15. As far as the pseudo-particle method is concerned, the equality is not perfectly satisfied, due to the approximation error from the pseudo-particle algorithm.

The complexity of the pseudo-particle method with quasi-periodic BCs stems not only from the decoupling of short- and long-range interactions but also from the notion of pseudo-particle rectangles and their sections, that are specific to each periodic domain image under consideration (see Fig. 11). Therefore, in order to verify the electrostatic force calculation for each particle, one can calculate the sum of all charges with which it interacts, including charges of actual particles, pseudo-particles, and pseudo-particle rectangle sections. For each particle this sum should be exactly equal to $(2N_{per} - 1)^3 N_p \times Q_p$ in the case of a mono-charged particle flow (same charge for every particle). This has been verified for the presented simulations, so the developed pseudo-particle algorithm and its extension for tri-periodic BCs is considered to be functioning according to its design.

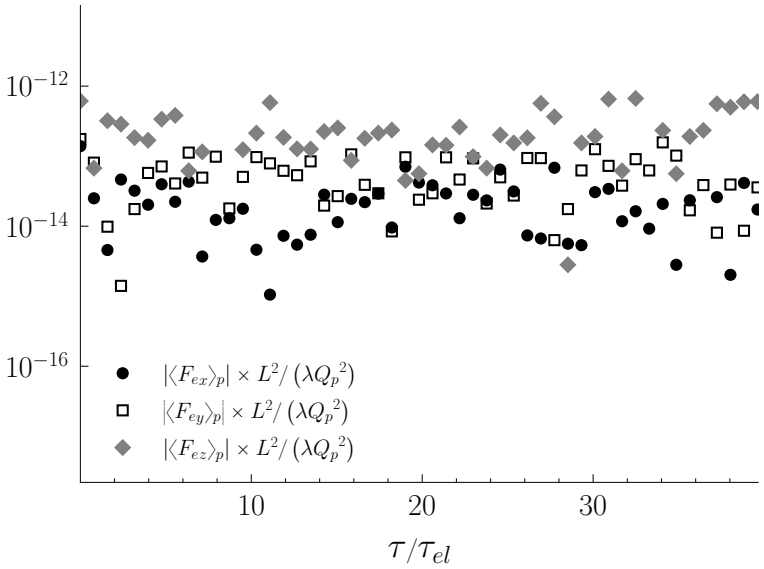

Fig. 15: *Verification of the calculation of electrostatic forces using the Direct method.*

2.4. Comparison of the numerical methods and configurations

Although the distribution of the approximation error $\epsilon_p^{N_e}(\mathbf{x}_p, t_0)$ seen in Fig. 14 provides a first comparison of pseudo-particle and direct method, in order to better understand how the impact of the different numerical methods on the simulated physics, one has to examine characteristic statistical moments calculated via simulations with different numerical methods/configurations.

To this end, several simulations of a dry mono-charged particle flow have been performed with $N_p = 10^4$ particles using Direct (DIR) and Pseudo-Particle (PS) algorithms with $N_{per} = 1$ quasi-periodic BCs. As stated in Subsect. 2.2, the number of cells N_e is dictated by the number of particles so as to have a desired average number of particles per cell N_k. For example, $N_k > 10$ would imply that $N_e < (N_p/10)^{1/3}$; for $N_p = 10^4$ this means that $N_e < 10$. Thus for simulations using the pseudo-particle algorithm, different numerical configurations are tested for $N_e = 4, 8$ and $N_v = 1, \ldots, N_v^{\max}$. For a given number of cells N_e, the maximum number of short-range neighbourhood cells, $N_v^{\max}$ is dictated by inequality (18). Table 2 contains $N_v^{\max}$ for increasing number of periodic layers N_{per} and various numbers of cells N_e.

To begin with, Fig. 16 shows the need for $N_v > 0$ in pseudo-particle algorithm, as it was previously stated in Subsect. 2.2 which underlines the importance of a high-fidelity calculation of short-range electrostatic interactions.

Table 2: *Maximum number of short-range neighbourhood cells* $N_v^{\max}$

N_e \ N_{per}	**1**	2	3
4	**1**	5	9
8	**3**	11	19

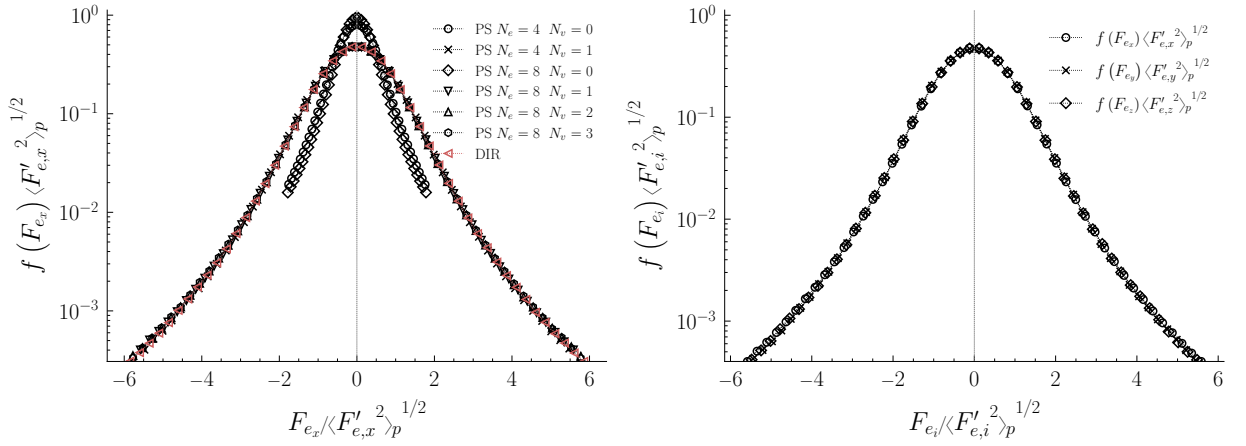

Fig. 16: *PDF of i-component of electrostatic forces. Left panel: Comparison of x-component for direct and pseudo-particle algorithm for various N_e with $N_v \geq 0$. Choice $N_v = 0$ should be avoided as it leads to a substantial error in the calculation of particle electrostatic forces due to an inaccurate calculation of the short-range electric field. Right panel: Comparison between all 3 components for the selected pseudo-particle algorithm with $N_e = 8$ and $N_v = 1$.*

It is observed that the PDF of electrostatic forces obtained with pseudo-particle algorithm and $N_v = 0$ is substantially different from the one obtained using direct method which is considered the high-fidelity reference simulation. The shape of the PDF of electrostatic forces for pseudo-particle algorithm with $N_v > 0$ matches the one obtained via the direct method. Apparently as number of cells N_e increases, a greater

Table 3: *Approximation error for different numerical algorithms/configurations*

Algorithm		$\langle\|\mathbf{F}_e\|\rangle_p/m_p$ $10^{-2}[ms^{-2}]$
PS	$N_e = 4$	4.0320
	$N_v = 1$	6.09%
PS	$N_e = 8$	3.9724
	$N_v = 1$	4.52%
PS	$N_e = 8$	3.8561
	$N_v = 2$	1.46%
PS	$N_e = 8$	3.8371
	$N_v = 3$	0.96%
DIR		**3.8007**

number of cells N_v is needed into the short-range neighbourhood as the cell size decreases in order to maintain the same neighbourhood size Δx_v. In Table 3 statistical moments of the particle flow are presented for different numerical algorithms/configurations. Their value using direct algorithm is considered as the value of reference and relative errors are calculated for each numerical configuration of the pseudo-particle algorithm. By choosing the values $N_e = 8$ and $N_v = 1$, the observed approximation error stays below 10% for $\sim 60\%$ of the particles as shown by Fig. 14. Considering the trade-off between the minimization of the approximation error and computational cost, it seems that this choice is reasonable for the simulations of $N_p = 10,000$ particles carried out in this work.

3. Numerical simulation of dry mono-charged particle flows

This section includes an analysis of numerical simulations of dry mono-charged particle flows that aims to characterize the particle-particle electrostatic interactions. It should be noted here, that according to [16] there is a saturation limit of surface charge density for small spheres, which can be translated (via d_p) to a corresponding limit for point-particle charges. For the configuration presented in this work, this value can be estimated to be approximately $4 \times 10^{-9}\ C$. The various particle charges that have been considered in all numerical simulations, all given in terms of a reference charge $Q_0 = 1 \times 10^{-9}\, C$ are of the same order of magnitude as seen in Table 4. In addition, in such simulations the calculation of electrostatic forces is

Table 4: *Properties of particle electrostatics*

Parameters	Symbol	Value	Units
Reference particle density	ρ_0	100	kg/m^3
Reference electric charge	Q_0	1×10^{-9}	C
Pseudo-particle cells	N_e	8	-
Number of neighbourhood cells	N_v	1	-
Number of periodic layers	N_{per}	1	-
Time-step	Δt	5×10^{-3}	s

very sensitive to numerical errors in particle position as $\|\mathbf{F}_e\| \propto 1/r^2$, since there is no dissipation. From an electrostatic dipole point of view, this means that an underestimation of the inter-particle distance would lead to an overestimation of electrostatic forces, which then leads to an overestimation of particle agitation, which would result in smaller inter-particle distance, and so on. In order to avoid this problem, but at the same time keep the effect of electric charges predominant in the simulated physics, we introduce a numerical dissipation that has been calibrated such that $\partial q_p^2/\partial t = 0$ in the stationary regime. That means adding the dissipative term $-\mathbf{u}_p/\tau_p$ in the right-hand side of Eq. (2), where $\tau_p = 650\tau_{el}$. In this way, that the physics of the simulation is predominantly controlled by electrostatic forces and not by this numerical dissipation. The characteristic time of electrostatic interactions τ_{el} can be estimated by dimensional analysis of Eq. (2) (see Appendix B).

3.1. Coulomb collisions and electrostatic interactions

To analyze the effects of the charges, one should define a characteristic time scale of electrostatic interactions. This time scale is the duration of particle velocity decorrelation under the sole presence of electrostatic interactions. The mechanism of this velocity decorrelation is the Coulomb collision as it has been defined in which is an elastic collision between two charged particles interacting with an effective Coulomb diameter d_{pq}^C, which is a notion typically found in cold plasma [17]. In the case of particle-laden flows, as seen in [18], the effective Coulomb diameter d_{pq}^C is defined as

$$d_{pq}^C = \lambda \frac{Q_p Q_q}{m_{pq} \langle \|\mathbf{w}_{pq}\| \rangle_p{}^2} \tag{21}$$

where the Lagrangian average of the norm of the relative particle velocity can be approximated by

$$\langle \|\mathbf{w}_{pq}\| \rangle_p = \sqrt{\frac{16}{\pi}\frac{2}{3}q_p^2}\ . \tag{22}$$

Additionally, $m_{pq} = m_p m_q / (m_p + m_q)$ is the reduced mass of a pair of particles p and q. If the kinetic energy of the particles is very large with regard to the electric potential energy, the deviation from the initial trajectories of the colliding particles is small. Therefore, $d_{pq}^C \leq d_p$ and particles would undergo a hard sphere collision, however the latter is not treated in our simulations. This length scale is also used to determine the size of the neighborhood Δx_v as it should be 10 times larger than the effective Coulomb diameter d_{pq}^C, $\Delta x_v \geq 10 d_{pq}^C$. Thus, for a given number of cells N_e, one can deduce the minimum number of cells $N_v^{\min}$ in the neighborhood of short-range interactions as

$$N_v^{\min} = \left\lceil \left(5\frac{N_e d_{pq}^C}{L} - \frac{1}{2} \right) \right\rceil\ .$$

3.2. Time-step sensitivity analysis

In order to perform simulations with adequate resolution of electrostatic interactions, the simulation time-step should be chosen such that the simulation can capture accurately the modification of particle trajectories. As a matter of fact, the most difficult task is the prediction of the trajectories of neighbouring approaching particles when the electrostatic forces and particle accelerations reach the largest values. In order to ensure an accurate prediction of the neighbouring particle trajectories and using the Coulomb collision representation, it is clear that the mean relative particle displacement during a time step $\delta l = \langle \|\mathbf{w}_{pq}\| \rangle_p \Delta t$ must remain significantly smaller than the effective Coulomb diameter d_{pq}^C.

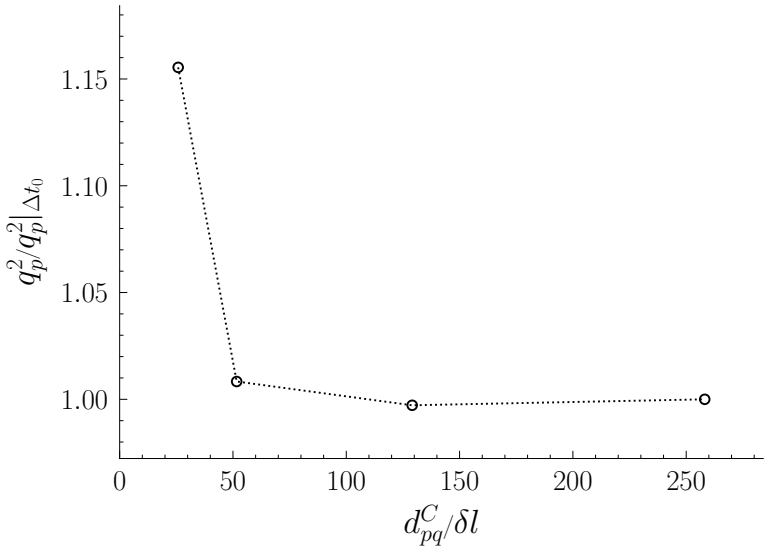

Fig. 17: *Convergence of the particle kinetic energy with respect to the Coulomb diameter normalized by the mean particle displacement for every time-step.* $\Delta t = 5 \times 10^{-3} s$ *is the minimum investigated time-step.*

Hence, the relevant parameter is $d_{pq}^C/\delta l$, leading to the definition of a particle CFL-like condition as,

$$\frac{\langle \|\mathbf{w}_{pq}\| \rangle_p \Delta t}{d_{pq}^C} \leq 0.01 \tag{23}$$

which allows to calculate a time-step threshold $\Delta t_{\max} \leq 0.01 \times d_{pq}^C / \langle \|\mathbf{w}_{pq}\| \rangle_p$, below which the resolution of electrostatic interactions is ensured. In any case, an inadequate time resolution seems to lead to a considerable overestimation of particle agitation as shown by Fig. 17. It is very interesting that if we replace d_{pq}^C from Eq. (21), the deduced expression for the time step coming from Eq. (23) is essentially the same as found in [19] following an energy equilibrium, which is an indication that the analogy between electrostatic interactions and (Coulomb) collisions is valid. It is clear that for particles of density $\rho_p = 2,750\ kg/m^3$, bearing charge $Q_p = 5 \times 10^{-9} C$, uniformly distributed in a domain of size $L = 2\pi\ m$, convergence is achieved for $d_{pq}^C/\delta l \sim 100$ at $\Delta t \leq 1 \times 10^{-2} s$ as seen in Table 5.

Table 5: *Time-step convergence*

Δt $10^{-3}[s]$	$d_{pq}^C/\delta l$	q_p^2 $10^{-3}[m^2 s^{-2}]$	$\langle \|\mathbf{F}_e\| \rangle_p / m_p$ $10^{-2}[m s^{-2}]$
50	25.82	5.2828 15.54%	3.8578 1.15%
25	51.63	4.6102 0.83%	3.8290 0.39%
10	129.09	4.5593 0.28%	3.8148 0.02%
5	**258.17**	**4.5721**	**3.8140**

3.3. Dimensional analysis

The characteristic time scale of Coulomb collisions is $\tau_{pq}^C = \left(n_p \pi {d_{pq}^C}^2 \langle \|\mathbf{w}_{pq}\| \rangle_p \right)^{-1}$. Using Eqs. (21) and (22), in mono-disperse mono-charged particle flows ($m_{pq} \sim m_p/2$ and ${Q_p}^2 {Q_q}^2 \sim {Q_p}^4$), the characteristic time of Coulomb collisions can be simplified to

$$\tau_{pq}^C \simeq \frac{1}{2} \frac{{m_p}^2}{\lambda^2 {Q_p}^4 n_p} \left(q_p^2\right)^{\frac{3}{2}} \ . \tag{24}$$

So, at this point a theoretical estimation for q_p^2 is needed in order to obtain one for τ_{pq}^C. To verify this, a numerical experiment is conducted, which consists of several simulations of mono-charged particle flows. We consider $Q_p = 5Q_0$, $m_p = 1.80 \times 10^{-4}\ kg$ and $n_p = 40.314\ m^{-3}$. Only one of the parameters Q_p, m_p, n_p is modified at a time, while the others are kept constant. The values for m_p can be deduced from those for ρ_p considering constant particle diameter d_p. Particle number density n_p depends both on the number of particles N_p and the domain size L. Therefore, keeping d_p and L constant, the values of parameters Q_p, ρ_p, N_p are chosen as $Q_p \in \{1,2,3,4,5,6\} \times Q_0$, $\rho_p \in \{200, 100, 50, 27.5, 15\} \times \rho_0$ and $N_p \in \{10, 25, 50, 100, 150\} \times 10^3$. For every simulation, the particle agitation q_p^2 is measured and an attempt is made to find a theoretical estimation based on dimensional analysis. Results are presented in Fig. 18.

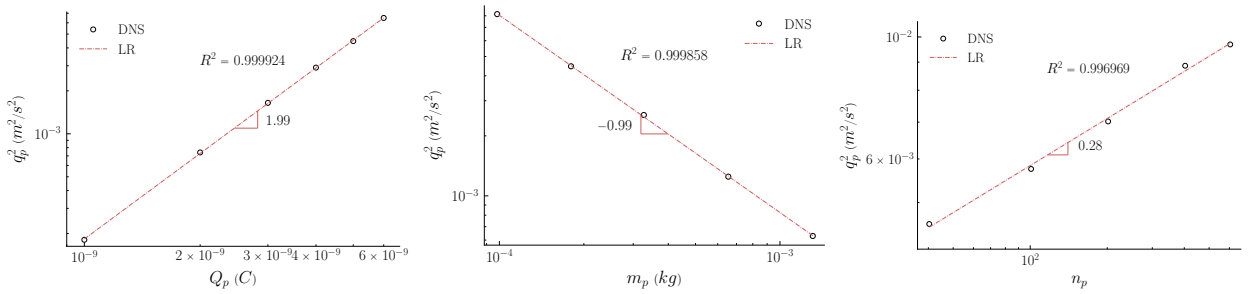

(a) $q_p^2 \propto {Q_p}^2$ **(b)** $q_p^2 \propto 1/m_p$ **(c)** $q_p^2 \propto {n_p}^{1/3}$

Fig. 18: *Particle agitation q_p^2 for mono-charged particle flows.*

This dimensional analysis shows that $q_p^2 \propto \lambda {Q_p}^2 {n_p}^{\frac{1}{3}} m_p^{-1}$. However, the coefficient in front of this term is determined as the slope of the linear regression of the measured q_p^2 for all simulations in Fig. 19.

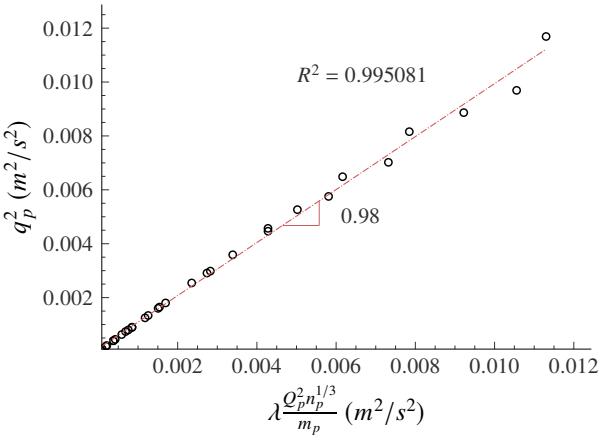

Fig. 19: *Particle agitation q_p^2 for all mono-charged particle flow simulations.*

That leads to the following theoretical relation for particle agitation in mono-charged particle flows

$$q_p^2 \simeq \lambda \frac{{Q_p}^2 {n_p}^{\frac{1}{3}}}{m_p} \ . \tag{25}$$

Replacing q_p^2 with its theoretical estimation from Eq. (25) to Eq. (24), gives an estimation of the characteristic time scale of Coulomb collisions as $\tau_{pq}^C = \frac{1}{2Q_p}\sqrt{\frac{m_p}{\lambda n_p}}$, which is in agreement with the result of Eq. (B.1). In order to verify this result via simple dimensional analysis, the Lagrangian particle integral time scale τ_p^t can be calculated for every simulation, as the integral of the Lagrangian autocorrelation function of particle velocity, $\tau_p^t = \int_0^\infty R_p(\tau) d\tau$, where $R_p(\tau) = \langle u'_{p,i}(t) u'_{p,i}(t+\tau) \rangle_p / 2q_p^2(t)$. Since in such a flow, particles move only due to inter-particle electrostatic interactions, it constitutes the characteristic time scale of electrostatic interactions. In this way, the effect of these parameters on τ_p^t can be isolated as shown by Fig. 20.

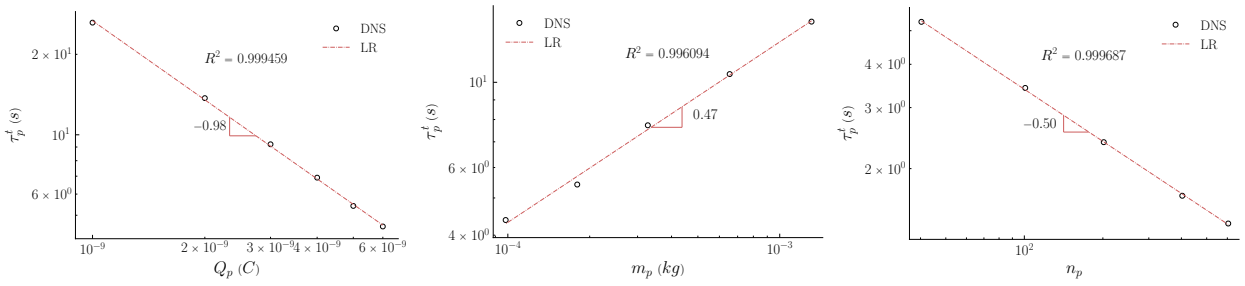

(a) $\tau_p^t \propto 1/Q_p$ **(b)** $\tau_p^t \propto \sqrt{m_p}$ **(c)** $\tau_p^t \propto 1/\sqrt{n_p}$

Fig. 20: *Lagrangian particle integral time scale τ_p^t for mono-charged particle flows.*

This dimensional analysis shows that $\tau_p^t \propto \lambda {n_p}^{-1/2} {Q_p}^{-1} {m_p}^{1/2}$, which verifies the theoretical analysis above. However, the coefficient is determined as the slope of the linear regression between the measured τ_p^t for all simulations in Fig. 21.

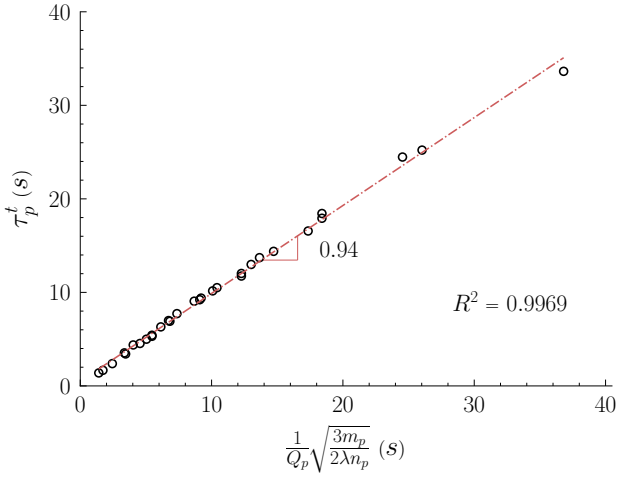

Fig. 21: *Lagrangian particle integral time scale τ_p^t for all mono-charged particle flow simulations.*

Consequently, we define the characteristic time scale of electrostatic interactions as

$$\tau_{el} = \sqrt{6}\tau_{pq}^C = \frac{1}{Q_p}\sqrt{\frac{3m_p}{2\lambda n_p}} \,. \tag{26}$$

This characteristic time scale can very useful when trying to model the effects of electrostatic interactions, as shown in [20]. Since the characteristic time of Coulomb collisions, τ_{pq}^C is of the same order of magnitude as τ_p^t for mono-charged particle flows, that means that Coulomb collisions is an adequate physical interpretation of inter-particle electrostatic interactions in this kind of flows. Finally, Eq. (21) can now be simplified by replacing $\langle \|\mathbf{w}_{pq}\| \rangle_p$ with its definition from Eq. (22) and consequently q_p^2 from Eq. (25) that leads to

$$d_{pq}^C \simeq \frac{3\pi}{16} {n_p}^{-\frac{1}{3}} \approx 0.589 {n_p}^{-\frac{1}{3}} \tag{27}$$

which is very close to the theoretical value of the average nearest-neighbor particle distance that derived analytically by [21] for a uniform particle distribution as $\langle d_{np} \rangle_p \approx 0.5539 {n_p}^{-1/3}$. This implies that the

effective Coulomb diameter in mono-charged particle flows does not depend on the particle mass for mono-charged particle flows. Although this is not straightforward, for such flows it can be explained by the fact that particle agitation q_p^2 depends solely on inter-particle electrostatic interactions. Lastly, this analysis also allows to make an estimation of the magnitude of electrostatic forces exerted on the particles, or equivalently of the particle acceleration due to electrostatic forces, $\mathbf{F}_e/m_p$. Its magnitude can be estimated using characteristic time and length scales which ultimately yields

$$\frac{\langle \|\mathbf{F}_e\| \rangle_p}{m_p} \simeq \frac{5}{2} q_p^2 {n_p}^{1/3} = \frac{5}{2} \lambda \frac{{Q_p}^2 {n_p}^{\frac{2}{3}}}{m_p} \tag{28}$$

as implied by simulation results presented in Fig. 22.

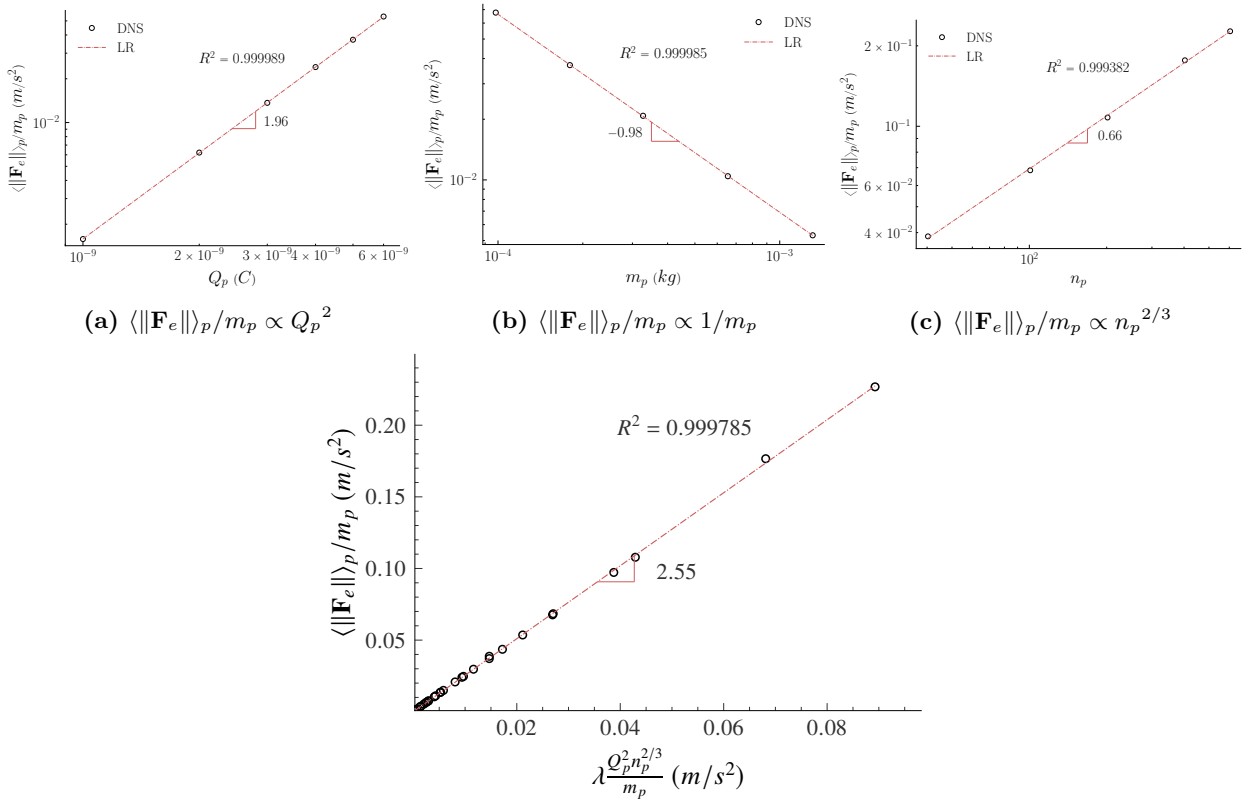

(a) $\langle \|\mathbf{F}_e\| \rangle_p/m_p \propto {Q_p}^2$ **(b)** $\langle \|\mathbf{F}_e\| \rangle_p/m_p \propto 1/m_p$ **(c)** $\langle \|\mathbf{F}_e\| \rangle_p/m_p \propto {n_p}^{2/3}$

(d) *all simulations*

Fig. 22: *Electrostatic particle acceleration* $\langle \|\mathbf{F}_e\| \rangle_p/m_p$ *for mono-charged particle flows.*

3.4. Particle motion due to particle-induced electric field

In a charged particle flow, the only source of kinetic energy is the electric potential energy stored in the system of particles due to their electric charge and initial position. Figure 23 shows an instantaneous snapshot of the mono-charged particle cloud where the velocities and electrostatic accelerations have been plotted for a qualitative appreciation of such a flow.

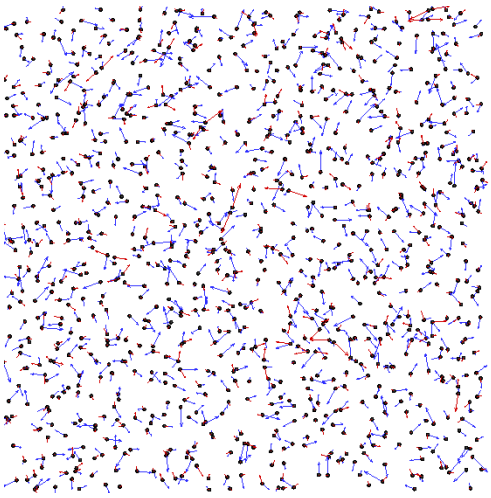

Fig. 23: *Instantaneous snapshot of a dry mono-charged particle cloud for* $\tau_{el} = 8.5s$ *and* $\Delta x = L/10$. *Particle velocities are depicted with blue color, while electrostatic forces with red.*

To get a better understanding of the physics of mono-charged particle flows, one can begin by examining particle agitation q_p^2. Figure 24 shows that for different levels of particle inertia, particle agitation follows an attenuated oscillation till it reaches a statistically steady value in the stationary regime. The observed oscillations are due to the expansion-contraction motion of the mono-charged particle cloud due to the combination of repulsive electrostatic forces (same-sign charges). However, at this point it is not evident if they are a numerical artifact of the quasi-periodic BCs.

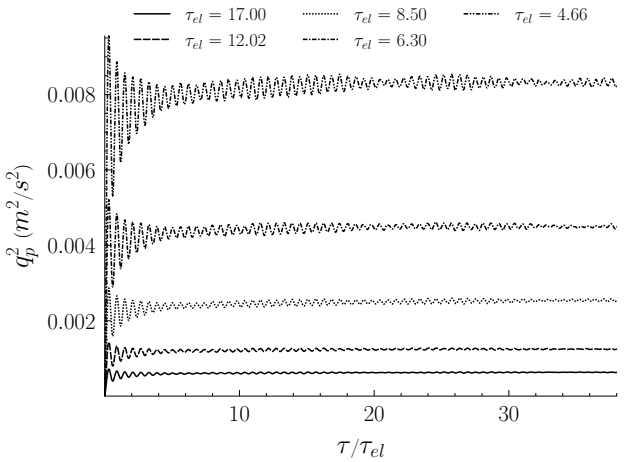

Fig. 24: *Time evolution of particle agitation for various levels of particle inertia.*

In the frame of the pdf approach for gas particle flows presented by [22], the equation of the variation of particle agitation q_p^2 can be written as

$$\frac{\partial}{\partial t} q_p^2 = \frac{\langle \mathbf{F}'_e . \mathbf{u}'_p \rangle_p}{m_p} \tag{29}$$

where the right-hand side $\langle \mathbf{F}'_e.\mathbf{u}'_p \rangle_p$ is the particle-induced electrostatic power, which in the case of charged dry particle flows is equal to the time derivative of the work of electrostatic forces. By performing a simple dimensional analysis, the particle-induced electrostatic power $\mathbf{F}_e.\mathbf{u}_p$ is proportional to the particle-induced electric potential ϕ $[V]$.

$$\mathbf{F}_e.\mathbf{u}_p \propto \frac{Q_p}{\tau_{el}} \times \phi(\mathbf{x}_p) \ .$$

The validity of the power balance in Eq. (29) is verified by Fig. 25 for various levels of particle inertia, where the same oscillation patterns are observed.

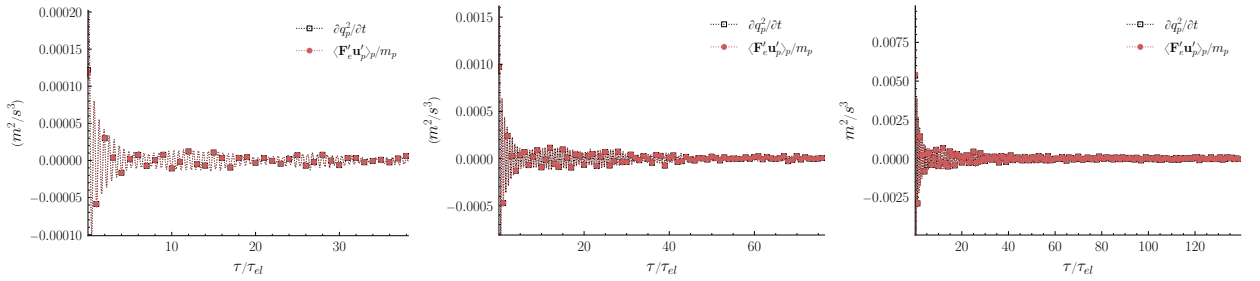

(a) $\tau_{el} = 17s$ **(b)** $\tau_{el} = 8.5s$ **(c)** $\tau_{el} = 4.66s$

Fig. 25: *Terms of Eq. (29) in transient regime for increasing particle inertia.*

In the stationary regime, $\partial q_p^2/\partial t = \langle \mathbf{F}'_e.\mathbf{u}'_p \rangle_p / m_p = 0$, which is in agreement with the minimum potential energy principle that is valid for conservative force fields, such as the electric field. According to this principle, the system of mono-charged particles is set to motion due to their initial electric potential energy (uniform initial position distribution), a part of which transfers to kinetic energy. Then, once the particles are set in motion, there is a constant transfer between kinetic and electric potential energy as particles approach and depart one from another. Such a system of particles, especially under the influence of a small dissipation, tends to a (statistical) equilibrium of minimum electric potential energy which implies that particles try to separate themselves as much as possible, albeit in constant motion.

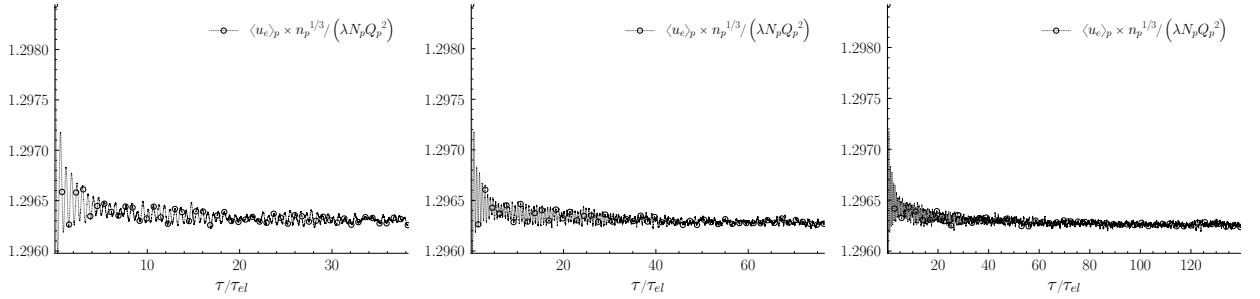

(a) $\tau_{el} = 17s$ **(b)** $\tau_{el} = 8.5s$ **(c)** $\tau_{el} = 4.66s$

Fig. 26: *Time evolution of normalized average electric potential for various levels of particle inertia.*

3.4.1. Particle-induced electric field and potential

The electrostatic force $\mathbf{F}_e$ exerted on a particle that lies within a system of N_p (electrostatically) charged particles is defined in Eq. (5) and the electric potential energy stored in a particle, u_e in Eq. (11).

Based on the latter, one could argue that for mono-charged particles electric potential can be indirectly calculated via the Lagrangian average of the electric potential energy normalized by the electric charge since $\langle\phi\rangle_p \sim \langle u_e\rangle_p / Q_p$. The particle-induced electric potential $\langle\phi\rangle_p$ is seen in Fig. 26. However, it seems to fail to capture the oscillations of the Lagrangian average of the electrostatic potential. We observe that $\langle\phi\rangle_p$ reaches a statistical steady value in the stationary regime. The time evolution of the Eulerian variance of the electric potential $\langle\phi'^2\rangle_p$ seen in Fig. 27 is more suitable as a criterion for the stationarity of the particle flow.

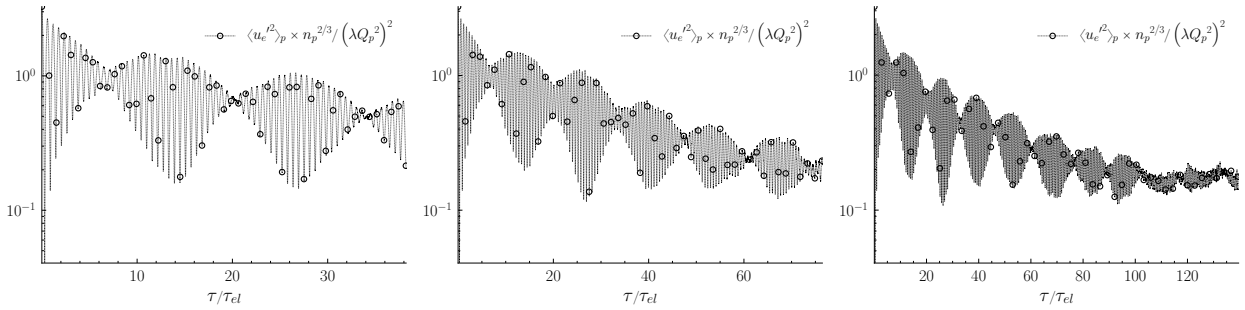

(a) $\tau_{el} = 17s$ **(b)** $\tau_{el} = 8.5s$ **(c)** $\tau_{el} = 4.66s$

Fig. 27: *Time evolution of normalized variance of electric potential* $\langle\phi'^2\rangle_p \times {d_{pq}^C}^2 / \left(\lambda Q_p\right)^2$ *for various levels of particle inertia. Simulations have been run for the same physical time, hence it takes considerably more time for heavy particles reach a steady state, as expected.*

4. Conclusion

In order to isolate electrostatic interactions, mono-charged dry particle clouds have been considered without the presence of any carrier fluid flow. Trying to calculate such electrostatic forces, especially considering tri-periodic boundary conditions, a challenging problem arises: that of electrostatic periodicity. More specifically, the successful application of electrostatic periodicity requires the ensuring both of the convergence and of the isotropy of the long-range electrostatic field. In order to address that, and at the same time consider the computational cost as well as the accuracy of the calculations, a rather efficient algorithm has been created and its characteristics as well as the obtained results are extensively analyzed and documented. Following, an attempt to explain the nature of electrostatic interactions is made via an analogy with hard collisions. In fact, particle-particle (repulsive) electrostatic interactions can be viewed as (Coulomb) collisions happening with an effective Coulomb diameter that is proportional to the square of electric charge and inversely proportional to the square of the norm of relative particle velocity. By considering this analogy, one can deduce a Coulomb collision frequency and consequently a characteristic

time scale of electrostatic interactions. A dimensional analysis supports this theory and it is verified via the corresponding measured quantities obtained by simulations of mono-charged particle-laden flows. Finally, particle agitation is linked to the particle-induced electric field and the very nature of electrostatic forces is observed in detail.

Declaration of interests

The authors report no conflict of interest.

Acknowledgements

The numerical simulations have been performed on supercomputer hosted by the meso-scale supercomputer center CALMIP as well as by the french national supercomputer center CINES.

References

[1] L. Greengard, The Numerical Solution of the N-Body Problem, Computers in Physics 4 (2) (1990) 142–152, publisher: American Institute of Physics.
[2] A. W. Appel, An efficient program for many-body simulation, SIAM Journal on Scientific and Statistical Computing 6 (1) (1985) 85–103.
[3] J. Barnes, P. Hut, A hierarchical $O(N \log N)$ force-calculation algorithm, Nature 324 (1986) 446–449. doi:10.1038/324446a0.
[4] L. van Dommelen, E. Rundensteiner, Fast, adaptive summation of point forces in the two-dimensional Poisson equation, Journal of Computational Physics 83 (1) (1989) 126–147.
[5] L. Greengard, V. Rokhlin, A fast algorithm for particle simulations, Journal of Computational Physics 73 (2) (1987) 325–348.
[6] R. W. Hockney, J. W. Eastwood, Computer simulation using particles, CRC Press, 2021.
[7] H. M. P. Couchman, Mesh-refined P3M-A fast adaptive N-body algorithm, The Astrophysical Journal 368 (1991) L23–L26.
[8] P. Ewald, Die Berechnung optischer und elektrostatischer Gitterpotentiale, Annalen der physik 369 (3) (1921) 253–287.
[9] J. W. Perram, H. G. Petersen, S. W. de Leeuw, An algorithm for the simulation of condensed matter which grows as the 3/2 power of the number of particles, Molecular Physics 65 (1988) 875–893.
[10] M. Deserno, C. Holm, How to mesh up Ewald sums. I. A theoretical and numerical comparison of various particle mesh routines, The Journal of Chemical Physics 109 (18) (1998) 7678–7693.
[11] M. Deserno, C. Holm, How to mesh up Ewald sums. II. An accurate error estimate for the particle–particle–particle-mesh algorithm, The Journal of Chemical Physics 109 (18) (1998) 7694–7701.
[12] J. Kolehmainen, A. Ozel, C. Boyce, S. Sundaresan, A hybrid approach to computing electrostatic forces in fluidized beds of charged particles, AIChE Journal 62 (7) (2016) 2282–2295. doi:10.1002/aic.15279.
[13] Y. Yao, J. Capecelatro, Competition between drag and coulomb interactions in turbulent particle-laden flows using a coupled-fluid–ewald-summation based approach, Physical Review Fluids 3 (3) (2018) 034301.
[14] H. Grosshans, M. Papalexandris, Direct numerical simulation of triboelectric charging in particle-laden turbulent channel flows, Journal of Fluid Mechanics 818 (2017) 465–491. doi:10.1017/jfm.2017.157.
[15] F. R. Bouchet, L. Hernquist, Cosmological simulations using the hierarchical tree method, The Astrophysical Journal Supplement Series 68 (1988) 521–538.
[16] N. Hamamoto, Y. Nakajima, T. Sato, Experimental discussion on maximum surface charge density of fine particles sustainable in normal atmosphere, Journal of Electrostatics 28 (2) (1992) 161–173.
[17] J. Callen, Fundamentals Of Plasma Physics, University of Wisconsin, 2003.
[18] A. Boutsikakis, P. Fede, A. Pedrono, O. Simonin, Numerical simulations of short-and long-range interaction forces in turbulent particle-laden gas flows, Flow, Turbulence and Combustion 105 (4) (2020) 989–1015.
[19] C. Bissinger, H. Grosshans, A new computational algorithm for the interaction between electrically charged particles, SN Applied Sciences 2 (5) (2020) 1–10.
[20] A. Boutsikakis, P. Fede, O. Simonin, Effect of electrostatic forces on the dispersion of like-charged solid particles transported by homogeneous isotropic turbulence, Journal of Fluid Mechanics 938 (2022).
[21] S. Chandrasekhar, Stochastic problems in physics and astronomy, Reviews of Modern Physics 15 (1) (1943) 1–89, publisher: American Physical Society.
[22] O. Simonin, Statistical and continuum modelling of turbulent reactive particulate flows, Lecture series 6 (2000).

Appendix A. Pseudo-particle algorithm

Appendix A.1. Pseudo-particle rectangles

A pseudo-particle rectangle X_k centered in position $\mathbf{x}_k^{eq}$ of equivalent pseudo-particle Ω_k, is defined in a cell whose center is denoted as $\mathbf{x}_k^c$. Its dimensions are $\mathbf{\Delta x}_k^{eq} = \mathbf{x}_{k\ \min}^{eq} - \mathbf{x}_{k\ \max}^{eq}$ where $\mathbf{x}_{k\ \min}^{eq}$ and $\mathbf{x}_{k\ \max}^{eq}$ are its borders.

$$x_{k,i_{\min}}^{eq} = \begin{cases} x_{k,i}^c - \dfrac{\Delta x_f}{2}, & \text{if} \quad x_{k,i}^{eq} < x_{k,i}^c \\ 2x_{k,i}^{eq} - x_{k,i}^c - \dfrac{\Delta x_f}{2}, & \text{otherwise} \end{cases} \tag{A.1}$$

and

$$x_{k,i_{\max}}^{eq} = \begin{cases} 2x_{k,i}^{eq} - x_{k,i}^c + \dfrac{\Delta x_f}{2}, & \text{if} \quad x_{k,i}^{eq} < x_{k,i}^c \\ x_{k,i}^c + \dfrac{\Delta x_f}{2}, & \text{otherwise} \end{cases} . \tag{A.2}$$

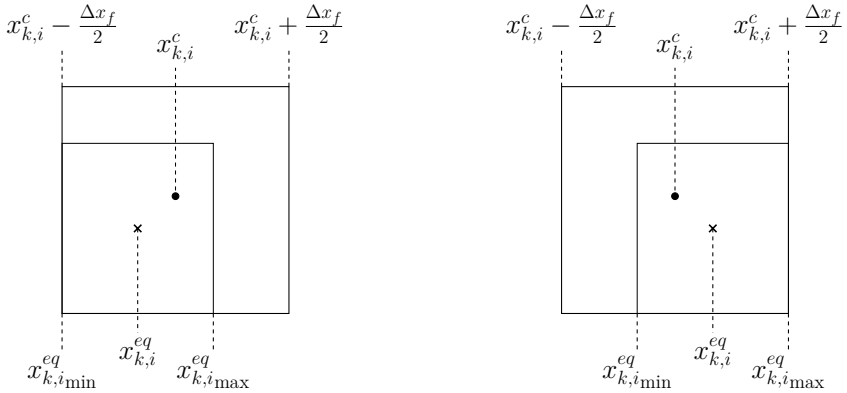

(a) $x_{k,i}^{eq} < x_{k,i}^c$ **(b)** $x_{k,i}^{eq} \geq x_{k,i}^c$

Fig. A.28: *Two different possible pseudo-particle positions* $\mathbf{x}_k^{eq}$ *relative to cell center* $\mathbf{x}_k^c$.

Appendix A.2. Optimal computational cost

The computational cost of the pseudo-particle algorithm with periodic boundary conditions depends on the number of particles N_p, the number of cells N_e, the number of neighborhood cells N_v and the number of periodic domain images N_{per}. Its function has been estimated theoretically in Eq. (20) and can be rewritten as

$$\mathcal{C}\left(N_p, N_e, N_v, N_{per}\right) = N_p \left[\left(2N_v + 1\right)^3 \frac{N_p}{{N_e}^3} + \left(2N_{per} - 1\right)^3 {N_e}^3 - \left(2N_v + 1\right)^3 - 1 \right] . \tag{A.3}$$

For given N_p, N_v and N_{per} there is an optimal number of cells $N_e^{opt} \in \left[\left(2N_v + 2\right) / \left(2N_{per} - 1\right), {N_p}^{1/3}\right]$ that minimizes the function of the computational cost. In order to calculate N_e^{opt}, one can write the partial derivative

$$\frac{\partial C}{\partial N_e} = -3{N_p}^2 \left(2N_v + 1\right)^3 {N_e}^{-4} + 3\left(2N_{per} - 1\right)^3 {N_e}^2 N_p \ . \tag{A.4}$$

Hence, N_e^{opt} is the solution of Eq. (A.4) with regards to N_e

$$\frac{\partial C}{\partial N_e} = 0 \Leftrightarrow N_p \left(2N_v + 1\right)^3 {N_e}^{-4} = \left(2N_{per} - 1\right)^3 {N_e}^2 \Leftrightarrow N_e^{opt} = {N_p}^{\frac{1}{6}} \left(\frac{2N_v + 1}{2N_{per} - 1}\right)^{\frac{1}{2}} .$$

If $N_n = \left(2N_v + 1\right)^3$ and $N_{im} = \left(2N_{per} - 1\right)^3$, then $N_e^{opt} = {N_p}^{1/6} \left(N_n / N_{im}\right)^{1/6}$ and the optimal (minimum) computational cost would be

$$\begin{aligned}
\mathcal{C}^{opt}\left(N_p, N_v, N_{per}\right) &= \mathcal{C}^{opt}\left(N_p, N_e^{opt}, N_v, N_{per}\right) \\
&= N_p \left[N_n \frac{N_p}{{N_p}^{\frac{1}{2}}} \left(\frac{N_{im}}{N_n}\right)^{\frac{1}{2}} + N_{im} {N_p}^{\frac{1}{2}} \left(\frac{N_n}{N_{im}}\right)^{\frac{1}{2}} - N_n - 1\right] \\
&= N_p \left[2N_n {N_p}^{\frac{1}{2}} N_{im} - N_n - 1\right] \\
&\sim {N_p}^{\frac{3}{2}} {N_v}^{\frac{3}{2}} {N_{per}}^{\frac{3}{2}}
\end{aligned}$$

and the corresponding optimal number of particles per cell is

$$N_k^{opt} = {N_p}^{\frac{1}{2}} \left(\frac{N_{im}}{N_n}\right)^{\frac{1}{2}} .$$

Appendix B. Nondimensionalization of the particle motion equation

In case of dry charged particle-laden gas flows with periodic boundary conditions, the equation of particle motion (2) can be written as

$$\frac{d\mathbf{u}_p}{dt} = \frac{1}{m_p} \sum_{\substack{q=1 \\ q \neq p}}^{N_p} \sum_{\substack{l,m,n=-N_{per} \\ |r^\dagger_{pq,i}| \leq \alpha_c}}^{N_{per}} \lambda \frac{Q_q Q_p}{\left\|\mathbf{r}^\dagger_{pq}\right\|^3} \mathbf{r}^\dagger_{pq} .$$

To nondimensionalize this equation, one should write every physical quantity q as $q = Q \cdot \tilde{q}$, where Q is a reference quantity and $\tilde{q}$ is the non-dimensional instance of quantity q. Table B.6, presents the quantities for the particle motion problem in charged particle flows. Finally by inserting the non-dimensional quantities

Table B.6: *Reference quantities for the particle motion problem*

Parameters	Symbol	Units
Length	L	m
Time	τ_{el}	s
Charge	Q_0	C
Mass	m_0	kg
Velocity	L/τ_{el}	m/s
Acceleration	$L/{\tau_{el}}^2$	m/s^2

in the equations one can get

$$\frac{L}{{\tau_{el}}^2}\frac{d\tilde{\mathbf{u}}_p}{d\tilde{t}} = \frac{1}{m_0}\cdot\frac{1}{\tilde{m}_p}\sum_{\substack{q=1\\q\neq p}}^{N_p}\sum_{\substack{l,m,n=-N_{per}\\|r^{\dagger}_{pq,i}|\leq\alpha_c}}^{N_{per}}\frac{\lambda{Q_0}^2}{L^2}\frac{\tilde{Q}_q\tilde{Q}_p}{\left\|\tilde{\mathbf{r}}^{\dagger}_{pq}\right\|^3}\tilde{\mathbf{r}}^{\dagger}_{pq}$$

$$\frac{d\tilde{\mathbf{u}}_p}{d\tilde{t}} = \frac{\lambda{Q_0}^2}{m_0L^2}\frac{{\tau_{el}}^2}{L}\cdot\frac{1}{\tilde{m}_p}\sum_{\substack{q=1\\q\neq p}}^{N_p}\sum_{\substack{l,m,n=-N_{per}\\|r^{\dagger}_{pq,i}|\leq\alpha_c}}^{N_{per}}\frac{\tilde{Q}_q\tilde{Q}_p}{\left\|\tilde{\mathbf{r}}^{\dagger}_{pq}\right\|^3}\tilde{\mathbf{r}}^{\dagger}_{pq}$$

$$\frac{d\tilde{\mathbf{u}}_p}{d\tilde{t}} = \frac{\lambda{Q_0}^2{\tau_{el}}^2N_p}{m_0L^3}\cdot\frac{\tilde{\mathbf{F}}_e}{\tilde{m}_p}\ .$$

This last equation is dimensionless and the ratio $\lambda N_p{Q_0}^2{\tau_{el}}^2/\left(m_0L^3\right)$ is also a dimensionless number. For a 1st order approximation, one could assume $\lambda N_p{Q_0}^2{\tau_{el}}^2/\left(m_0L^3\right)\sim 1$, which yields

$$\tau_{el}\propto\frac{1}{Q_0}\sqrt{\frac{m_0}{\lambda n_p}}\ . \tag{B.1}$$